Vysoké učení technické v Brně
Fakulta strojního inženýrství
Ústav konstruování

Brno University of Technology
Faculty of Mechanical Engineering
Institute of Machine and Industrial Design

MAGNETORHEOLOGICAL STRUT FOR VIBRATION ISOLATION SYSTEM OF SPACE LAUNCHER

Ing. Ondřej Macháček
Autor práce
Author

doc. Ing. Ivan Mazůrek, CSc
Vedoucí práce
Supervisor

Zkrácená verze disertační práce
Shortened Version of the Dissertation Thesis

Brno 2018

ABSTRACT

The dissertation thesis deals with the design of magnetorheological (MR) strut for vibration isolation system (VIS) of the space launch vehicle. Previously used VIS and their struts are described in state of the art. Each of the struts which contained any fluid was sealed by static seals and elastic bellows made of steel. The strut of a passive system called ELVIS was chosen as an inspiration and therefore analysed thoroughly. The strut is three-parametric that means the damper is elastically connected. The stiffness of this connection is identical to the projection of bellows volumetric stiffness into the axial direction which is called the pressure thrust stiffness.

The method of the pressure thrust stiffness determination from bellows dimensions presented in the thesis. Moreover, the parameters which can be used for the modification of the ratio between axial and pressure thrust stiffness of the bellows. This ratio affects the dynamic behaviour of the strut, thus also the behaviour of whole VIS.

The multi-body model of VIS based on the Stewart platform mechanism and detailed multi-body model of a single strut was created for the prediction of their dynamic behaviour in a vibration environment. Simulations have revealed the parameters which affect the efficiency of the MR strut: the time response and the dynamic force range of the MR valve. The range of these parameters which should ensure an effective vibration isolation by the MR strut in the specific VIS was determined by the multi-body model; specifically, time response: *0-5 ms* and the dynamic force range *5-10*.

The final design of the MR strut for the VIS of the launch vehicle preceded the design, manufacture and testing of the experimental strut. The parameters of the experimental strut were measured and consequently used for the verification of models used in the thesis. Knowledge obtained during the tests were used in the final design of the strut. One of the most important detections was that the ferrite (material used in the magnetic circuit) cracked during the semi-active control of the experimental strut. Therefore, a method of the fast magnetic circuit designing was established and subsequently patented. The method is based on a shape modification of the magnetic circuit which ensures shorter time response and the magnetic circuit is manufactured by 3D printing. The MR strut designed in this thesis has a predicted time response of *1.2 ms* and dynamic range *10*. The method which was used for the design process is summarised in conclusions.

KEYWORDS

vibration isolation system, launch vehicle, payload adapter, magnetorheological, damper, strut, valve, vibrations, suspension, damping, isolation, elastically connected damper, short time response, pressure thrust stiffness, metal bellows

CONTENT

1 INTRODUCTION

Spacecraft is one of the most sophisticated things in of these days. It is used for communication, navigation, research etc. Currently used spacecrafts have made significant progress in comparison with the first one - Sputnik (launch in 1957), unlike launch vehicles. Especially the principle of the launch vehicle traction stays almost the same for more than 50 years.

The vibration environment is much harder than the on-orbit vibration environment. Although the spacecraft spends most of the lifetime on orbit, its components are dimensioned for the flight vibration environment, which takes only around 5 minutes. This approach leads to the high weight of the spacecraft components thus high mission costs, because transport of 1 kg to low orbit cost from 4 000 – 40 000 USD, depends on the total weight of the payload [1].

Vibration isolation system usually made of aluminium or composite is inserted between the sensitive payload (spacecraft) and the booster which is the main source of the vibrations. However, sometimes reduce the vibration transmissibility is a priority. This happened, for example, in the transport of the Hubble Telescope [2]. Thus, the vibration isolation system used in this mission was more efficient, but also heavier compared to other flights.

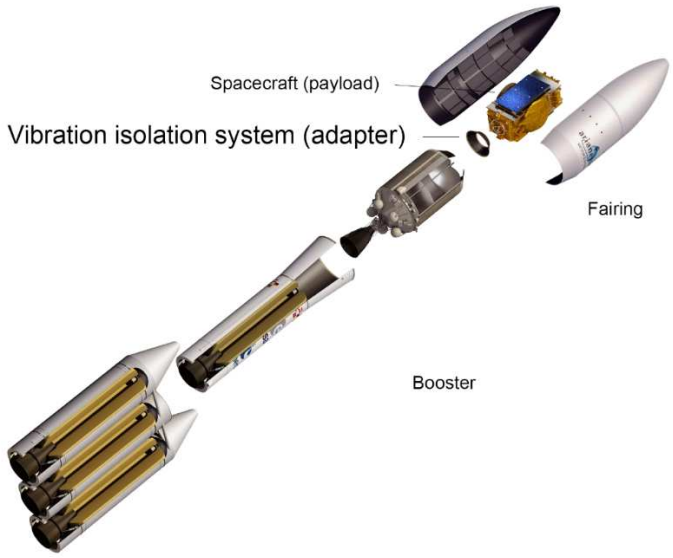

Fig. 1 Concept of launch vehicle Ariane 6 (ESA) [3]

Even more payload comfort can be achieved by active vibration elimination. However, the weight of active vibration isolation system designed for spacecraft Artemis was approximately 5 times higher than the passive adapter intended for the same flight [4]. The weight increase was caused especially by the power supply and other electrical equipment.

A perfect vibration isolation system would be lightweight and very effective. This thesis examines the possibility of using semi-active vibration isolation system based on magnetorheological damper which efficiency is much higher than passive dampers. The power consumption of such as damper is in watts, so it could not increase the weight of the vibration isolation system significantly.

2 STATE OF THE ART

2.1 Vibration isolation systems for the space application

Vibration isolation systems (VIS) are used in launch vehicle to decrease of vibration transmissibility between excitation body (launch vehicle) and sprung mass (payload). Acceleration bellow (blue signal in Fig. 2) and above (yellow signal) the VIS was measured during the launch vehicle Taurus (NASA) flight [6]. Vibrations and shocks are most often formed by booster oscillation, fairing separation of by lift-off blastwave. The payload must resist (to stay undamaged) in this vibration environment.

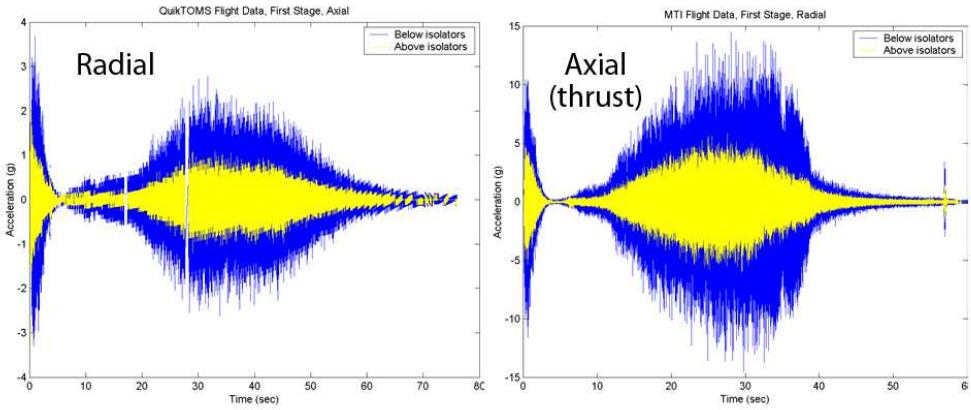

Fig. 2 Taurus/GFO flight data, bellow and above isolators [6]

VIS can be divided by application to whole spacecraft VIS or satellite part VIS (antennas, optical equipment etc.). The main difference between these two groups is their lifetime. Whole spacecraft vibration isolation is necessary only during the flight – separating of the satellite (payload) from the launch vehicle happens approximately 5 minutes after the start. On the other hand, the satellites VIS has to ensure On-orbit vibration isolation which usually takes several years.

2.1.1 Structural vibration isolation systems

Usually passive systems which isolate the vibrations by the suitably designed shape of their structure. The SoftRide products belong to this group. The Uniflex and the Omniflex systems were developed to isolate frequency lower than *80 Hz*. Higher frequencies can be isolated for example by ShockRing which reduces vibration most effectively around *1 kHz* [7]. Cone made of composite material is the most common element for launch vehicle payload vibration protection in ESA. This structural VIS are sometimes called payload adapter.
The adapter diameters are normalized. The lower (base) diameter corresponds to the connection with the launch vehicle, diameter 2624 mm is used in Ariane 5, *1920 mm* in Vega, *2000 mm* in Soyuz *2000 mm*, etc. The upper diameter depends on the payload which is used. Launch vehicles user manuals defined these upper (payload) diameters: *937, 1194, 1663, 1666* a *2624 mm* [8].

However, not just the dimensions have to be kept, another important parameter is the natural frequency of the system consists of payload and adapter. The payload modal shapes may disturb the flight control (sampling frequency is usually 50 Hz). Therefore, there is a request to keep the natural frequency of the system within the range *20 – 45 Hz* in the longitudinal direction. The natural frequency in lateral direction has to be higher than *7.5 Hz*, this value is relevant for a payload mass *6 500 kg*. Thy system with a payload lighter than *2 500 kg* has to have a frequency higher than 15 *Hz*.

Fig. 3 ESA adapters: PAS 937C (left) [8] a PAS 1194C (right) [9]

2.1.2 Mechanical vibration isolation systems

Vibration energy spreads in all directions, therefore the Stewart platform (6 DOF mechanisms) is used almost exclusively [5, 10, 11]. The Stewart platforms have various numbers of struts. But, at least 6 struts guarantee 6 DOF mechanisms. The strut may consist of spring and damper [5], actuator [12] or both [11].

Evolved launch vibration isolation system (ELVIS)

Passive system ELVIS was tested with experimental payload, which had similar geometric parameters to parameters of commonly used satellite.

Lateral excitation was provided by dynamometer with harmonic movement: with a constant amplitude of stroke *5 mm* up to frequency *10 Hz* and constant amplitude of acceleration *1* g for the frequencies higher than *10 Hz*. Accelerometers were connected to the payload at various position, their amplitude-frequency dependency is shown in Fig. 4.

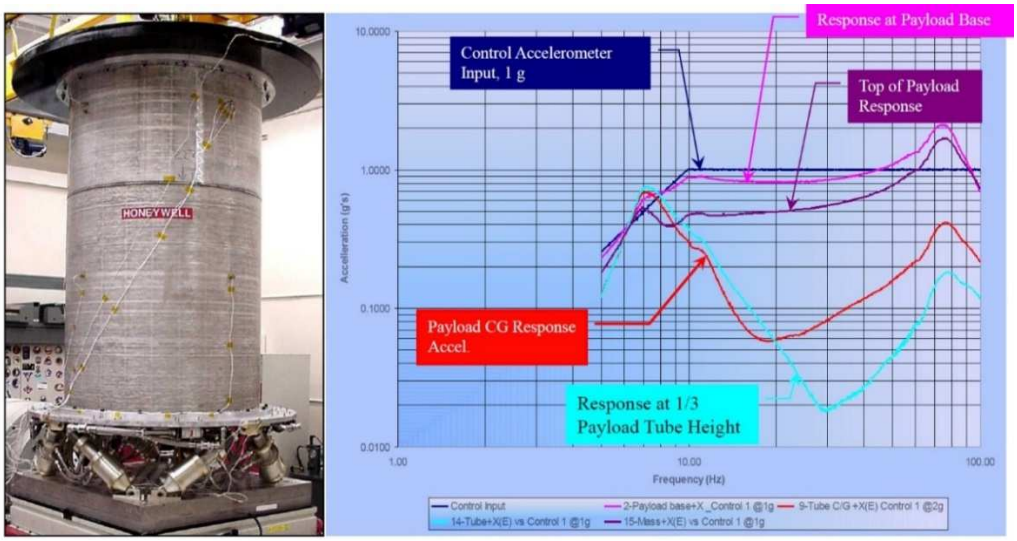

Fig. 4 ELVIS and acceleration measured in the lateral direction [5]

The acceleration signals revealed the presence of two modal shapes in range *5 – 100 Hz*. The payload behaviour can be estimated due to that the accelerometers were fixed in the various height of payload. The low-frequency acceleration peak (around *7 Hz*) has a similar shape along the whole payload height. Of which it can be concluded that the translation movement was dominant for this modal shape. On the other hand, transmissibility of high-frequency peak (around *70 Hz*) differs significantly along the payload height. This modal shape was probably similar to the rotation with the axis of rotation near the point with the lower transmissibility. This point is approximately in a third of height by measurement, see blue curve in Fig. 4.

2.2 Struts of VIS for space application

The strut of mechanical VIS combines a function of spring and damper. The spring accumulates the vibration energy and it is necessary to payload support. The damper dissipates the kinetic energy of the vibration and it is necessary to decrease of vibration amplitude in the vicinity of resonance.

2.2.1 The strut of the ELVIS

This strut is also inspired by the D-strut, the main difference is that strut of ELVIS uses just one pair of bellows with the same stiffness in instead of two pairs in D –strut with primary and secondary stiffness. The fluid flows between the bellows due to the hole in the piston rod. The pressure in the fluid cannot stretch the secondary bellows. Nevertheless, this concept is also called three-parametric, because the pressure causes “inflating” of bellows.

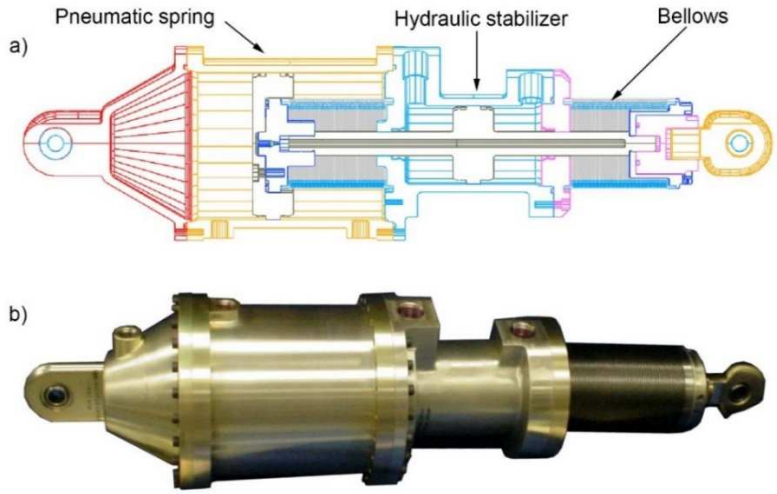

Fig. 5 Scheme a) and photo b) of ELVIS strut [5]

Davis defines the resistance against this deformation as volumetric stiffness [13]. However, this stiffness is marginal in his conception with respect to the difference in orders between the volumetric stiffness and axial stiffness of the secondary bellow. The volumetric stiffness cannot be neglected in the strut of ELVIS. The value of volumetric stiffness is the key parameter to the stiffness determination of the damper elastic connection.

The primary stiffness of the strut is formed by the axial stiffness of primary bellows and a stiffness of pneumatic spring. The pressure in chambers of the pneumatic spring is equal under the static load of the strut [5]. The difference between the effective area above and below the piston of pneumatic spring multiplied by the pressure inside the chambers defines the static load of the strut. The various pressure in the spring allows using this strut for various sprung mass with the same compression of the strut. The bellows are not preloaded in this position.

The strut of ELVIS is innovative in the solution of elastically connected damper by pressure thrust stiffness of bellows. The disadvantage of this concept is that the pressure thrust stiffness is not listed in datasheets of bellows. Therefore, the chose of the bellows for this application is complicated. Without known, the pressure thrust stiffness cannot be guaranteed the strut functionality. Therefore, next chapter will be focused on the elastic metal bellows and determination of its parameters.

2.3 Metal bellows

Metal bellows are the commonly used for thermal expansion in pipelines – loaded by axial force; for a component of the clutch – loaded by torsion, or for pressure accumulators – loaded by internal pressure. However, the bellows can be used as the case of damping fluid.

A leakage of a fluid has destructive effects on electronics of spacecraft (payload). Damper with conventionally sealing placed between the piston rod and body of the damper is prone to leakage because the sealing is between parts whit relative movement. Dynamic sealing of piston rod can be replaced by static sealing of flexible bellows. The leakage risk of static sealing is much lower than the risk of a dynamic one. Moreover, the static type of sealing has no friction, which brings benefits in the dynamic behaviour of semi-actively damped system.

Fig. 6 Formed and welded bellows [15]

Axial stiffness of bellows is much lower than a resistance against the volume change caused by internal pressure. The volume change is accompanied by the length change in axial direction – pressure thrust stiffness. Axial stiffness commonly available in product lists, while the pressure thrust stiffness is not. Final Element Analysis (FEA) is one of a possible approach is to determining the pressure thrust stiffness using the bellows dimensions and parameters.

2.3.1 FEA of metal bellows

Above mentioned shell parts were simulated by many authors [16 - 18]. The FEA used two general approaches:

3D model meshed by “SHELL“ elements [17]
2D model with axial symmetry meshed by “SOLID“ elements [16]

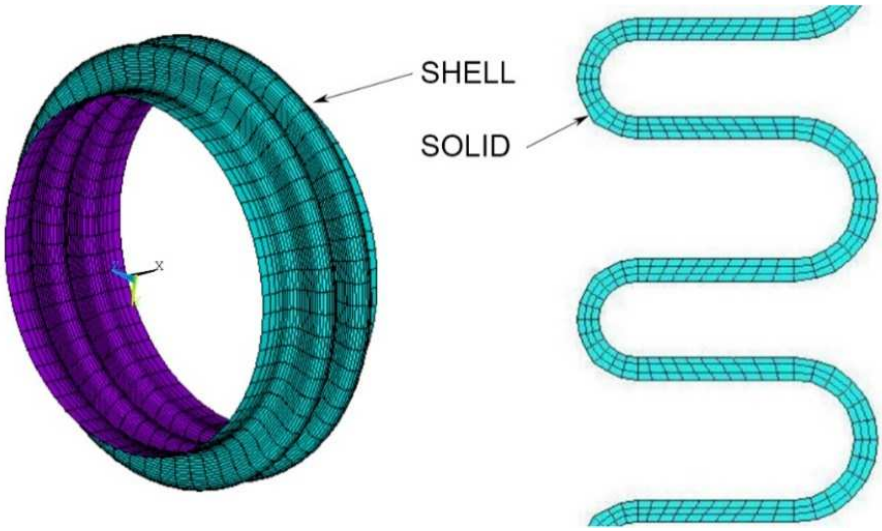

Fig. 7 3D shell and 2D solid model of metal bellows [18]

Thakkar compared both methods in his dissertation thesis [18], the difference between these approaches is shown in Fig. 7. Moreover, the results are compared with the analytical counting. The stresses obtained by both approaches of FEAs are almost the same. In addition, consistent with the results obtained analytical, the deviation is approximately *20 %*.

Search in the literature did not reveal any FEA of metal bellows deals with the interaction between the filling of the bellows and the wall. However, there were some mentions that the internal pressure causes the length deformation of pipelines. It is caused by the pressure forcing on the surface between the minimum and maximum diameter of bellows. This force is called pressure thrust [19].

2.4 Magnetorheological dampers

Research in this field was started in 1939 [20]. However, application of the MR effect occurred at the end of 20th century. The conventional design of MR damper contains a gap in the piston, see Fig. 8. The magnetic field can be applied in the gap using an electromagnetic coil. The ferromagnetic particles of the MRF fluid are dispersed randomly and the damping in this state is not high. But, when the coil is powered by an electric current, magnetic flux density in the gap increase, the particles are formed into a chain-like structure, the yield stress of the fluid increase and the damping force in this state is significantly higher than the force at inactivated state.

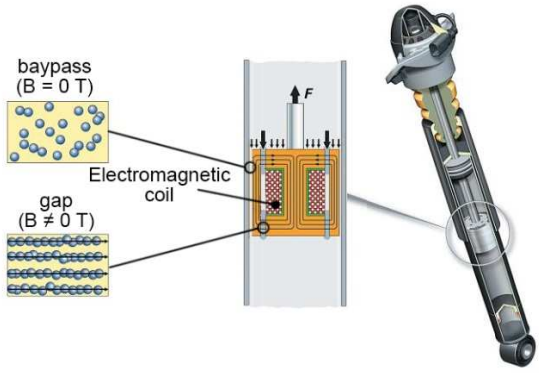

Fig. 8 MR damper with the magnetic circuit in piston [21]

2.4.1 Dynamic force range of MR dampers

Magnetic field influenced the MR damper force. Therefore, the force-velocity dependency of the MR damper has to be measured for various magnetic flux density in the gap that means various current in the coil of the damper. Dynamic force range – one of a performance parameter of MR damper is defined by ratio between thr damping force generated with maximum magnetic flux density in the gap $F_{max}(v,B)$ and the damping force generated with minimum magnetic flux density in the gap $F_{min}(v)$ [22]:

$$D(v_0) = \frac{F_{max}(v_0)}{F_{min}(v_0)} = \frac{F_\tau(\tau_{max}) + F_\eta(v_0) + F_f}{F_\eta(v_0) + F_f} = 1 + \frac{F_\tau(\tau_{max})}{F_\eta(v_0) + F_f} \qquad (1)$$

Dimensions of channels which affected the damping force are usually designed using analytical counting base on a so-called parallel plate model, see Fig. 9. The model considers the fluid flow between two parallel plates; the geometry is similar to flowing through the gap of the MR damper [22].

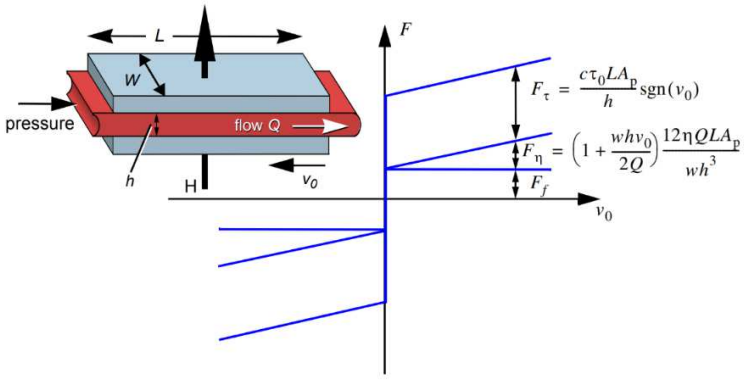

Fig. 9 Forces component of the MR damper [22]

Where:
- F_f is friction force created by seals, guiding, etc.
- F_η is viscous force created by the internal friction of the fluid, $A_p = (\pi/4)\cdot(D\text{-}d)^2$ is an effective area, which is given by the piston D and piston rod d diameters. The viscous force is dependent on the piston velocity v_0
- F_τ is force necessary to overcome the yield stress of MR fluid τ_0, the force can be control by the electric current in the coil Coefficient c is within the range 2.07 to 3.07 [23]

2.4.2 The response time of MR dampers

Semi-active controlled damper performance is given by time period which is necessary to change of damping force – time response. The force increases nonlinearly, see Fig. 10 a). Thus, it is complicated to determine the time between changes of the force from minimum to maximum. Therefore, the time response is reported as time between 0 to 62.3% of maximum value [24, [2525] – the primary response or 0 to 95% [22, 26] – the secondary response.

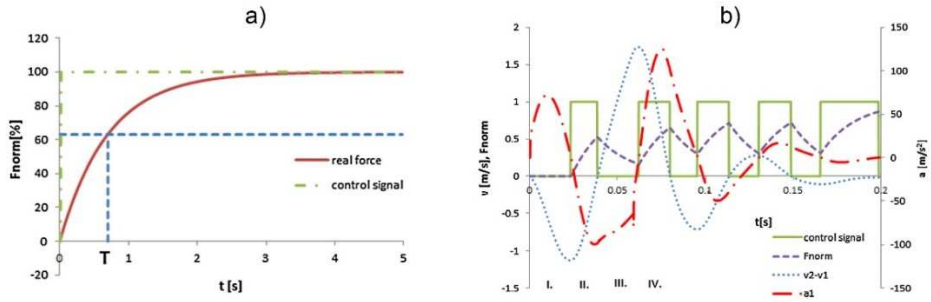

Fig. 10 The response time of MR damper and simulated signals [25]

Total time response of MR damper is influenced by time of current rise, which can be significantly shortened by current [22]; time response of MR fluid itself [24, [27]; and eddy currents which are generated in the coil core [25]. The influence of eddy effect on the MR damper time response depends on the geometry and material of magnetic circuit (coil core).

The eddy currents flow in the perpendicular direction to the magnetic field and they are inducted by magnetic flux density changes [28]. The currents are always closed in loops. These loops generate a secondary magnetic field which has opposite direction to the magnetic field, which causes the eddy currents.

There are two different approaches to prevent forming of eddy currents: **material approach** using composite materials for example sintered ferrites of Soft Material Composites (SMC) [29]; or **shape approach** using laminated coil cores [30]. The eddy current loop is not able to cross the insulating layer on the border of metal sheets, see Fig. 10 a) or insulating film in the case of composite material, see Fig. 10 b). The smaller size of loops the lower effect of the eddy currents that result in shorter time response of MR damper.

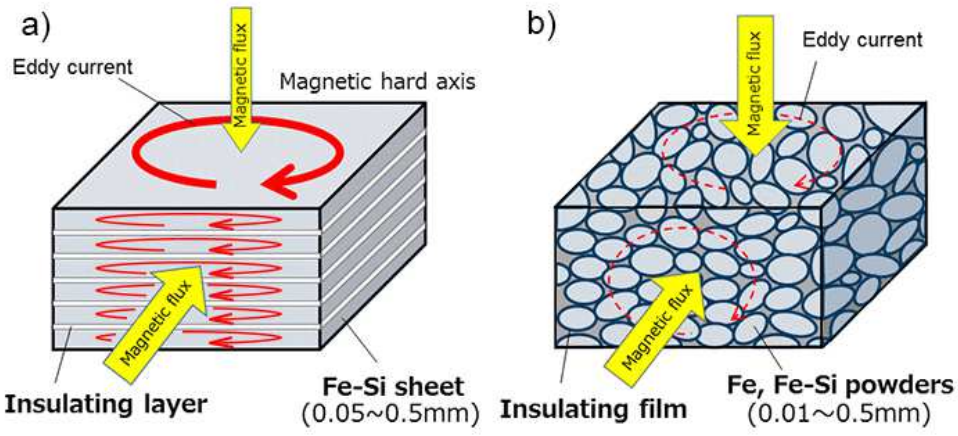

Fig. 11 Eddy currents in magnetic core a) laminated b) composite [31]

2.4.3 MR damper for the space application

One of the few MR dampers, which were designed for space application, was patented in 2005 [32]. This damper, more precisely strut or an isolator, because of certain stiffness, has internal MR valve and there is no piston rod for a guiding as it is common.

Piston movement of the damper causes the fluid flow. There are two possible paths of flow from the outer chamber to the inner one: the first through two gaps with coil along the housing or directly through only one gap and bypass, see in Fig. 12. Both paths cause high damping.

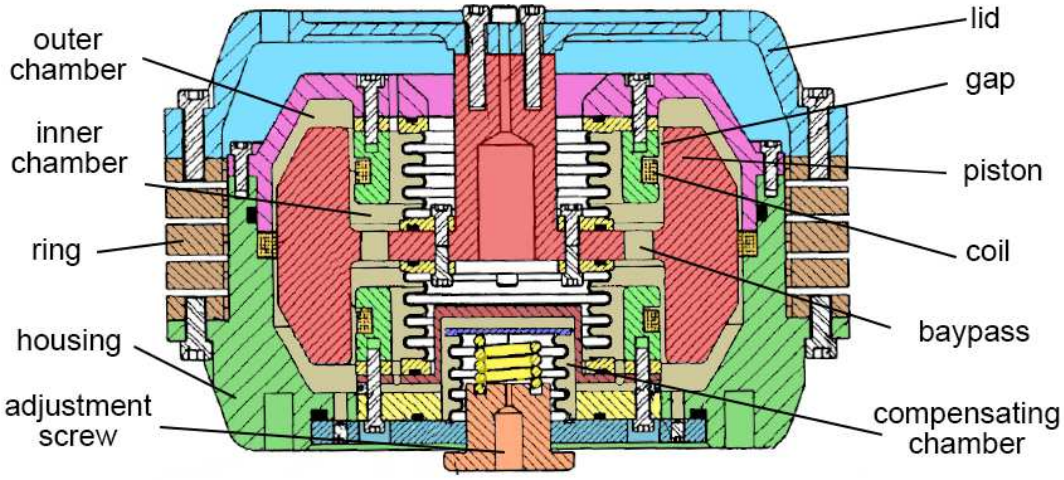

Fig. 12 The response time of MR damper and the influence of response time on semi-active control [32]

An elimination thermal expansion is provided by metal bellows which creates a compensating chamber. The bellows is connected by adjustment screw to set a required pressure inside the damper.

The lid serves to the guidance of the piston because the upper part of the lid is weakened what results in elastic deformation in the axial direction, while the stiffness of the lid lateral direction is much higher. Therefore the isolator can be considered single-axis and it is designed for low stroke applications. The absence of dynamic seals and guidance guarantees no friction force, what should result in high dynamic force range in low piston velocities. Semi-active controlled damper with high dynamic force range is effective by Yang [22].

3 CONCLUSIONS OF LITERATURE REVIEW

The vibration environment during a flight of the launch vehicle is very dangerous for the valuable payload (spacecraft). Two basic types of vibration isolation systems (VIS) were used for the space application: mechanical and structural. Mechanical VISs were used with passive (whole spacecraft isolation) or active (light part of the spacecraft) control.

Single axis elements such as actuators, struts etc. used for vibration elimination must be united in a mechanism with 6 DOF. A literature review points out the Stewart platform as the best candidate. It is usually consists of 6 actuators and this active mechanism, is used also for positioning of light mass devices. However, it was found the passive platform whose legs are struts, which operate and spring and damper. One of such as the designed passive Stewart platform is called ELVIS.

All strut used for the space applications which was filled with a fluid was sealed by elastic metal bellows and some static seals. Conventional sealing by dynamic seals between the piston rod and a damper body are not allowed in this field, because a leaked fluid would evaporate due to atmospheric pressure drop. Consequently, condensation of the vapour on the spacecraft electronic parts, short circuit, which may endanger the mission.

Available literature didn't provide any information on how to determine the volumetric stiffness of metal bellows neither the pressure thrust stiffness (projection of volumetric stiffness into the axial direction). The pressure thrust stiffness determination is necessary for the strut design. Therefore, FEA will be used for the pressure thrust stiffness determination using the bellows geometry.

Suspension system employing the MR damper with the parameters lying in this area will be able to significantly decrease the transmissibility of vibration in comparison with the suspension system using the MR damper with one or both parameters out of this rectangle.

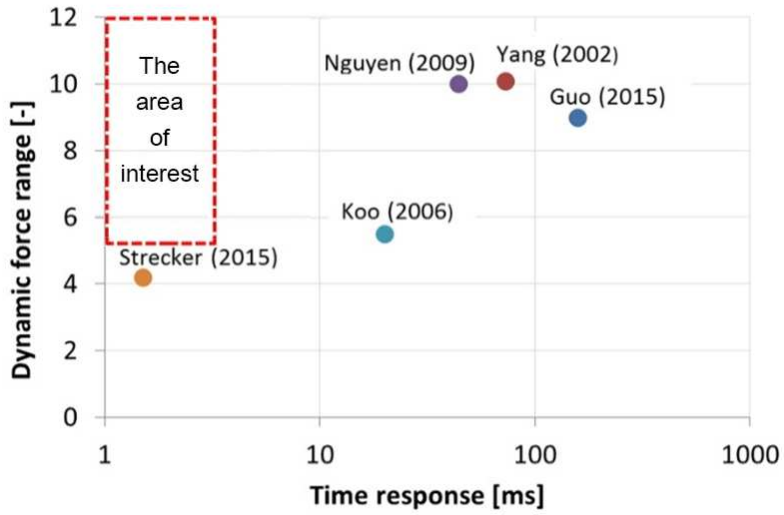

Fig. 13 Time response – Dynamic force range dependency of existing MR dampers

4 AIM OF THE THESIS

Vibration isolation system for the launch vehicle is a complex task. This thesis is focused on the design of key element of the vibration isolation system.

The aim of the thesis:
Design of semi-active strut combining spring and damper function for the vibration isolation system of the launch vehicle.

Sub-aims:

- Multi-body modes of vibration isolation system and strut
- Hydraulic, pneumatic and magnetic analysis for the optimal strut dimensioning
- Design and manufacture of an experimental strut for laboratory testing
- Verification the experimental strut functionality during vibration tests
- Design of the strut for VIS of the launch vehicle

Methods:
Multi-body model of the single strut will be used to define the area of interest for the MR strut, see Fig. 13. The model will be verified by experiment. The MR strut will be designed in two versions:

Experimental: verification of the multi-body model of the strut
Final: use in the VIS of the launch vehicle

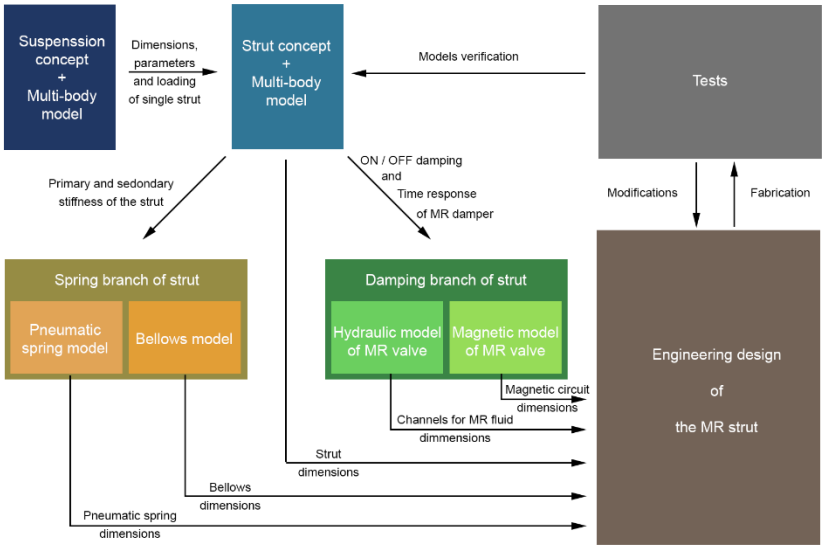

Fig. 14 Scheme of MR strut design process

Design process will used many models and calculations for optimal dimensioning of the strut. Inputs outputs and interconnection of the models and other procedures during the design process is shown in Fig. 14.

The strut dimensioning is based on the whole VIS requirements: payload mass $m = 1\ 500\ kg$, centre of gravity height $h_{CoG} = 1.5\ m$. VIS + payload natural frequency: $3 – 25\ Hz$ (lateral), $8 – 45\ Hz$ (axial). Max. displacement of the payload $30\ mm$ (lateral), $10\ mm$ (axial).

5 DESIGN OF MR STRUT

5.1 Conceptual design of MR strut

The literature review described some struts used previously for the purpose of vibration isolation for space application. The strut of ELVIS was chosen as the most suitable source of inspiration for the new MR strut. The pneumatic spring will ensure the dominant part of the primary stiffness of the MR strut. This spring is suitable especially for the possibility of the pressure regulation and for the equal pressure under and above the piston in static load created by payload in gravitation field *1 g*.

Axial stiffness of metal bellows will contribute the primary stiffness of the strut. Moreover, these flexible parts will serve as the case of the damping medium – MR fluid. Thus, the conventional piston rod seals will not use, because of higher friction and a risk of leakage in comparison of metal bellows sealed by static seals.

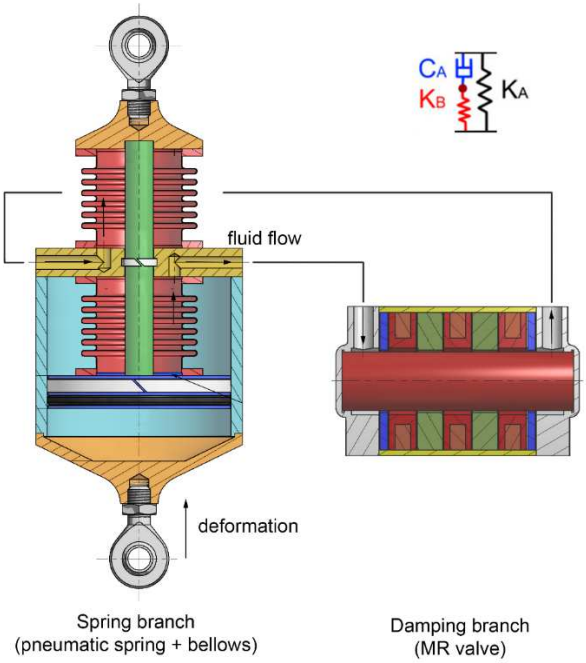

Fig. 15 Conceptual design of the MR strut

5.2 Dimensions and parameters determination of VIS and strut

Force affecting on each strut was determined by solving of the system of motion laws solution. The payload behaviour on the Stewart platform was simulated by the model in multi-body system ADAMS. A complex model of vibration isolation system was operated only in passive mode and with linear elements, that means the stiffness and damping of the strut were constant. More sophisticated simulation such as semi-active control was provided in detail model of the strut, especially for lower time requirements. Also, the verification by measurement can be provided much easier with a model of the single strut. However, boundary conditions were determined in the model of VIS.

5.2.1

5.2.1 Multi-body model of VIS

Multi-body model of VIS consists of two rigid bodies, which are interconnected by 8 struts and a mechanical stabilizer. Lower (green) body - base represents the launch vehicle, thus the source of vibration with acceleration $\ddot{x}_0$. Upper (yellow) body represents a payload and the response on the excitation is measured by the acceleration of payload $\ddot{x}$.

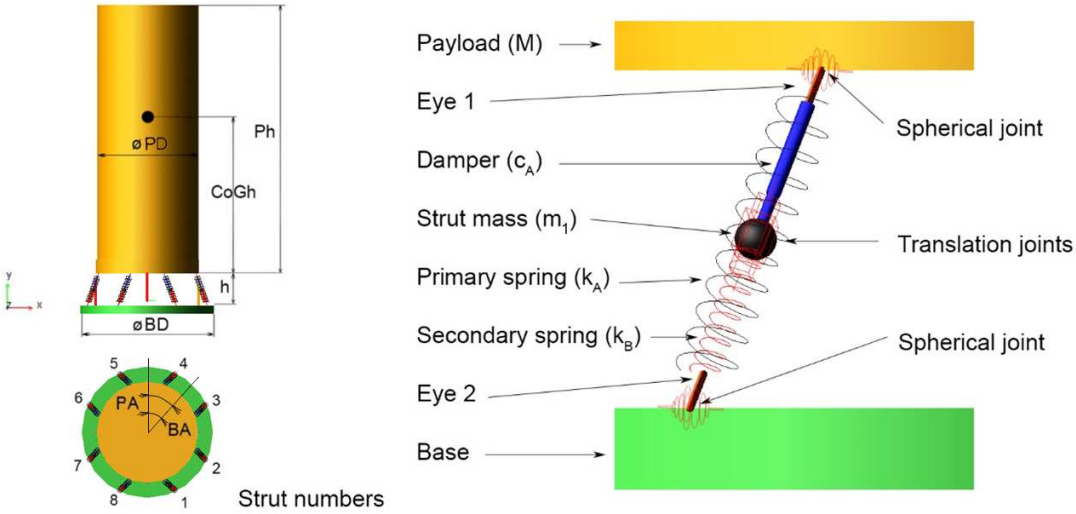

Fig. 16 Scheme of VIS multi-body model

Parameters of Stewart platform which meet the required transfer ratio for payload of mass *M = 1500 kg* and dimeter *PD = 1 280 mm* are*:* base diameter *BD = 1 660 mm*, angle between the struts along the payload perimeter *PA = 19°*, angle between struts along the payload perimeter *BA = 26°*, platform height *h = 400 mm*. The strut has the primary stiffness k_A *= 1 230 N/mm*, the secondary stiffness is approximately 50 times higher *N = kB/kA = 50* and the strut damping is c_A *= 26 Ns/mm*. Transfer function of the VIS and payload is plotted in Fig. 17 by transfer ratio in different height of payload for lateral vibration and only in centre of gravity for axial vibration.

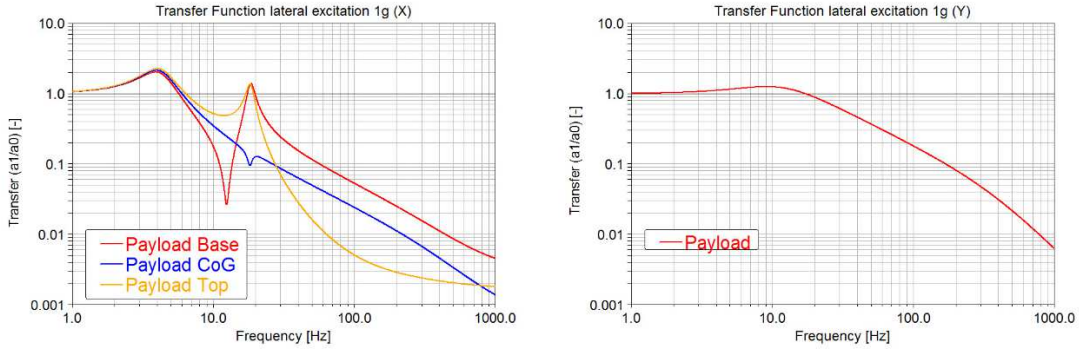

Fig. 17 Transmissibility function of the VIS + the payload system

The maximum strut deformation is given by the superposition of quasi-static and dynamic excitation and it is around *17 mm*. So, a stroke of the strut with this value of (constant) stiffness should be *20 mm*.

The payload displacement during dynamic (lateral) and quasi-static (axial) excitation is within the permissible range. Payload displacement at the top during quasi-static load in axial direction exceeds the limit a little. However, progressive force-deformation dependency of pneumatic spring should decrease this maximum of payload displacement under the *10 mm* which is the limit.

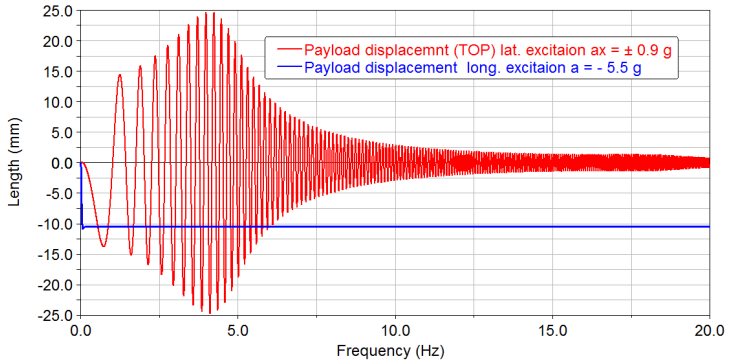

Fig. 18 Payload displacement during dynamic (lat.) and quasi-static (ax.) load

Load of the strut for its dimensioning

Maximum strut force is able to determine only in the case when the excitation is well known. But the vibration environment in the launch vehicle can be predicted just roughly. Therefore, the maximum strut force was obtained as the sum of force caused by the quasi-static acceleration in axial direction *5.5 g* and maximum damping force during harmonic excitation of acceleration in a lateral direction with amplitude *0.9 g*. Consequently, the sum was multiple by safety factor *2*.

tab. 1 Limit forces of the MR strut

Parameter	Symbol	Value	Unit
Quasi-static force in the strut (5.5g)	$F_{5.5g}$	11.9	[kN]
Damping force	F_C	5.06	[kN]
Total strut force	F_{SDE}	33.92	[kN]

5.2.2 Multi-body model of single

The boundary conditions of the single strut model are based on the axial excitation of the VIS multi-body model. 8 struts with an inclination relative to the base plate are replaced by a single strut in the axial direction. Thus, the payload mass for experimental strut was chosen *100 kg*. The stiffness and damping of the experimental strut were chosen so that the transmissibility was similar to the VIS + payload system, see right side of Fig. 17.

Multi-body model of single strut consists of three bodies: base (where the excitation is applied) payload, (where the response is measured) and m_1, which represents the mass of moving parts of the damper. This body is connected with payload by damper c_A and with the base by spring k_1.

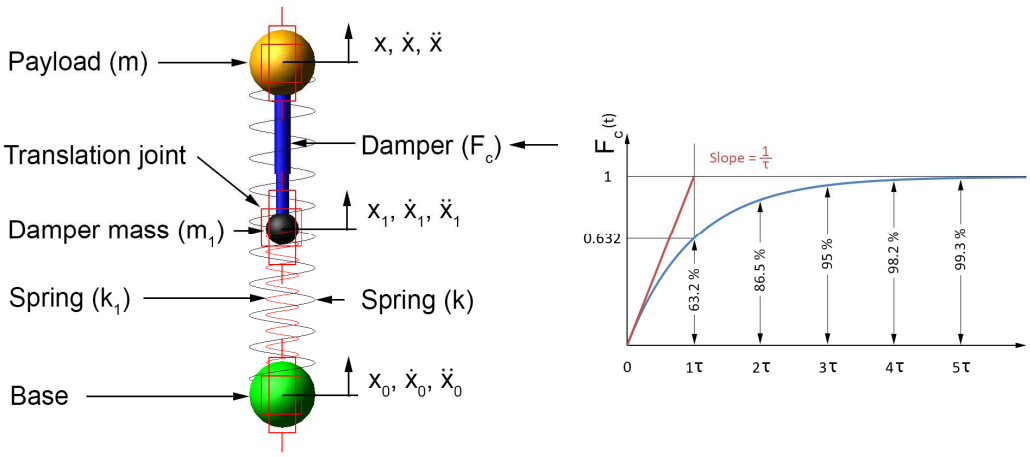

Fig. 19 Scheme of single strut model

Parameters of the single strut model were determined by the VIS simulations on $m = 100\ kg$, $k = 400\ N/mm$, $C_{ON} = 12.5\ Ns/mm$ and $k1 = 50*k$. Effect of time response and dynamic force range of MR valve in semi-active control mode is described below. The base is excited by the axial acceleration of amplitude *1 g*. Frequency increases linearly from *0* to *100 Hz*, simulation time was *100 s* and number of steps *400 000*.

Time response

A time delay of damping force increase was inserted into the model to observe the behaviour of the mass during the semi-active control of the strut. The force increasing is similar to the response of the first order system, see in the right side of Fig. 19. Damping force can be control by the semi-active algorithm. The position of the damper between the payload and the body m_1 caused slight changes of equations, for the ON/OFF Skyhook algorithm:

$$\begin{aligned} \dot{x} \cdot (\dot{x} - \dot{x}_1) \geq 0 \ &\rightarrow Fc = Fc_{max} \\ \dot{x} \cdot (\dot{x} - \dot{x}_1) < 0 \ &\rightarrow Fc = Fc_{min} \end{aligned} \tag{2}$$

Acceleration of the payload and the base were transfer into the frequency spectra using Fast Fourier Transformation (FFT) and the amplitudes of both signals were divided for the same frequencies. This calculation results in “transmissibility function”. However, considering that thy system is not linear, the designation as the function is not clear. Therefore, “the transfer ratio” will be used:

$$T(f) = \frac{\ddot{x}(f)}{\ddot{x}_0(f)} \tag{3}$$

The dependency of time response on the transfer ratio is shown in Fig. 20. Simulation confirmed the hypothesis that the time response increase results in the higher amount of vibration transfer onto the sprung mass by the semi-active controlled strut. The system behaviour at the frequencies higher than in this case from 5*0 Hz* is distorted by the fact that the excitation was harmonic. Thus, the damping of the damper with slow time response for example *10 ms* has stabilized on a specific value which results in lower transfer ratio than the ratio achieved by semi-actively controlled

damper with faster response, for example, *2 ms*. However, this "advantage" of slower damper would probably not be confirmed in the case of real excitation, for random vibration. A significant benefit of semi-active control was observed for the dampers with the time response lower than *5 ms*. A system with the damper with time response *10 ms* has similar transfer ratio in the vicinity of resonance in compare of passive mode. Therefore, the time response of the MR strut should be lower than *5 ms*.

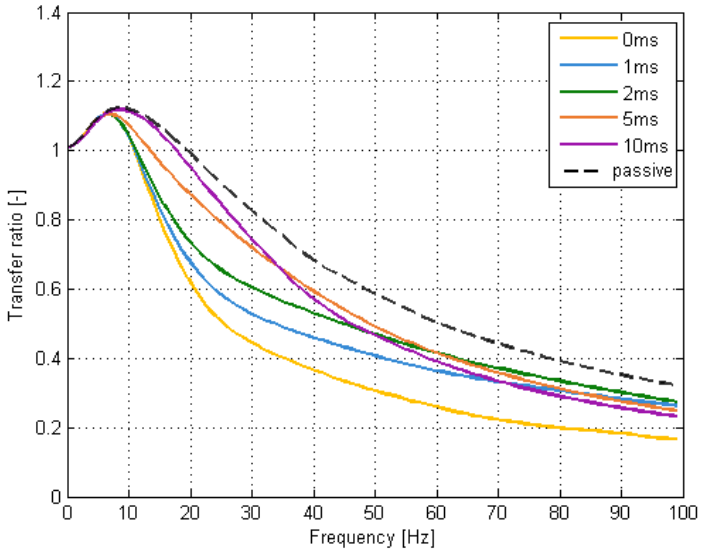

Fig. 20 Influence of time response on the transfer ratio

Dynamic force range

Simulations deals with the dynamic force range were provided with the constant damping in ON state. The value of dynamic range affects just the damping in OFF state. Results in Fig. 21 show that the transfer ratio of the system equipped with damper with dynamic force range *D = 50* is similar than the transfer ratio of the system with the damper with dynamic force range infinitely high.

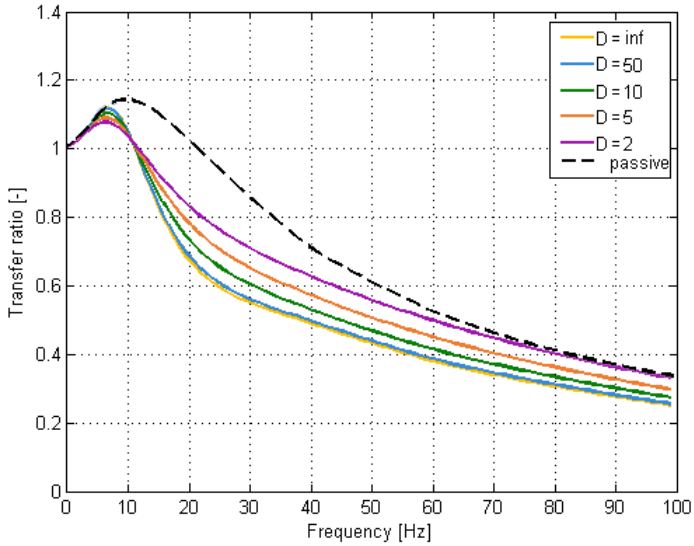

Fig. 21 Influence of dynamic force range on the transfer ratio

Dynamic force range increase causes a significant decrease of the transfer ratio at isolation area, but also a slight increase in the vicinity of the resonance. This handicap of semi-active control can be mitigated by the proportional control of the damping force. That means to use an algorithm which switches between more than two levels of damping as the ON/OFF Skyhook.

Dynamic range higher than *5* proves to be suitable for this system as suitable, because, the transfer ratio was significantly lower than the transfer ratio achieved by passive damping. However, the dynamic force increased over the value *10* has minimal benefit onto the transfer ratio. Therefore, the dynamic range of the MR strut should be between *5* and *10*.

5.3 Experimental MR strut design

The functionality verification of MR strut is necessary before the final design of MR strut for space application. Therefore, the experimental strut was manufactured and tested. Moreover, some vibration experiments with the experimental strut were used for verification of multi-body model described in chap. 5.2.2. The experimental strut consists of two coil springs, bellows unit, and an external magnetorheological valve. This strut was inserted into the system (demonstrator) which is illustrated in Fig. 22. Excitation is provided by the hydraulic actuator; sprung mass is realized by a set of weights. The sprung mass and actuator are connected by the experimental strut. Therefore, the transmissibility of the experimental strut can be determined by measurement of acceleration bellow (actuator) $\ddot{x}_0$ and above (sprung mass) $\ddot{x}$ the strut.

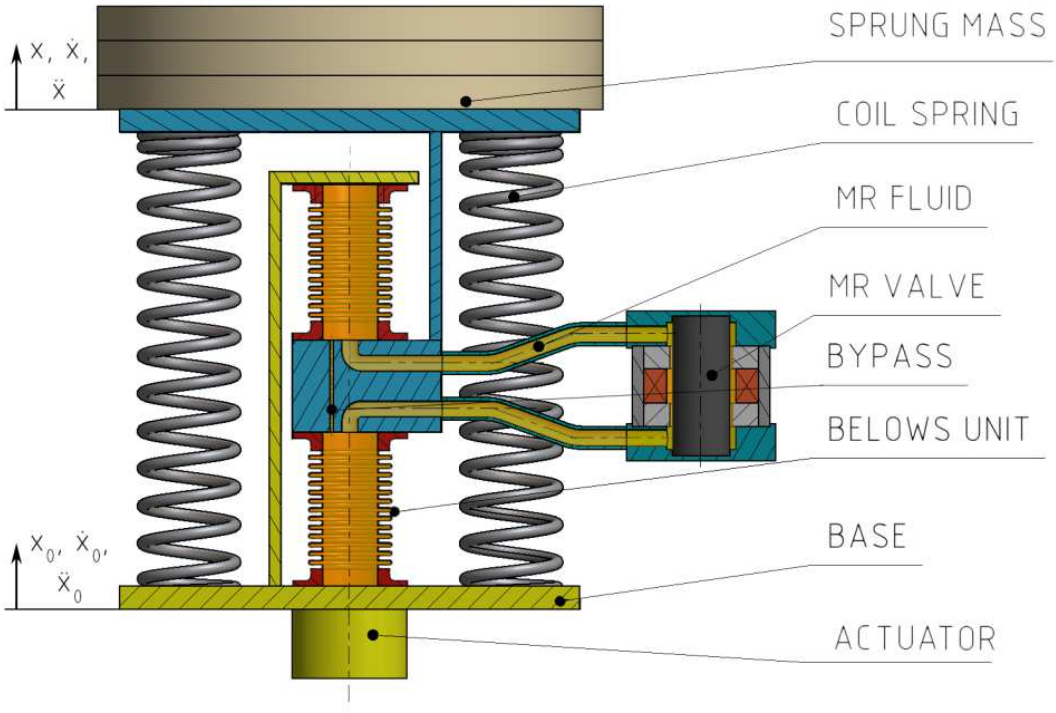

Fig. 22 Experimental strut in the demonstrator

5.3.1 Demonstrator of the experimental MR strut

Parts of bellows unit, MR valve, weights, etc. were manufactured and assembled in accordance with the scheme in Fig. 22. The bellows unit is in Fig. 23 shown without the sheets, which connected the lids and without the frame, because of greater clarity. MR valve is equipped with the pressure sensor *HBM 154210274* and the valve which is used to connect the expansion tank, which is necessary to easy change of the pressure inside the experimental strut.

Fig. 23 Important parts of the experimental MR strut

Both components of MR strut shown in Fig. 23 were separately filled with the MR fluid and then interconnected by steel tubes. After that, the MR strut was deaerated. The steel tubes were used because of higher volumetric stiffness in compare with the rubber hoses, which were planned to use originally.

Fig. 24 Demonstrator for the experimental strut vibration isolation properties verification

Excitation is realized by a hydraulic dynamometer (actuator), which displacement was set that its acceleration was constant *1 g* in a whole range of tested frequencies. The acceleration was measured by accelerometer *B&K 4507B* screwed to the base, see detail at the bottom right of Fig. 24. The same sensor was placed on the sprung mass. The ratio of these two signals gives a transmissibility of the experimental strut. Position sensor *VLP 15 SA 150* was inserted between the base and the sprung mass. The relative velocity between these two bodies was calculated by derivation of the position signal.

5.3.2 Experimental verification of the strut parameters

Force-velocity dependency determination requires a force measurement. Therefore, the load cell *INTERFACE 1730ACK-50kN* was inserted between the frame and the sprung mass, see Fig. 25. Velocity was determined by the position sensor signal derivation.

Fig. 25 Demonstrator configuration for the F-v dependency measurement

tab. 1 Measured parameters of the demonstrator

Parameter	Symbol	Value	Unit
Sprung mass	m	95.6	[kg]
Primary stiffness	k	395	[N/mm]
Secondary stiffness	k_1	2844	[N/mm]
Damping in ON state (I = 1 A)	C_{ON}	non-linear	[Ns/mm]
Damping in OFF state (I = 0 A)	C_{OFF}	non-linear	[Ns/mm]
Time response	T	4	[ms]
Dynamic force range (maximum)	D	9	[-]

5.3.3 Transfer ratio of the demonstrator

Vibration isolation strut cannot be evaluated only by parameters, which are measured separately but verify its behaviour in the complex system. That means to determine the transfer ratio – amplitude of vibrations transmitted from the vibration source to the sprung mass. Therefore, the strut was inserted into the complex system (demonstrator) and the transfer ratio was measured.

Passive mode of MR valve has been used for the most of tests. In Fig. 26 there are three of them for the currents *0 A*, *0.5 A* and *1 A* together with the simulation results (dashed lines).

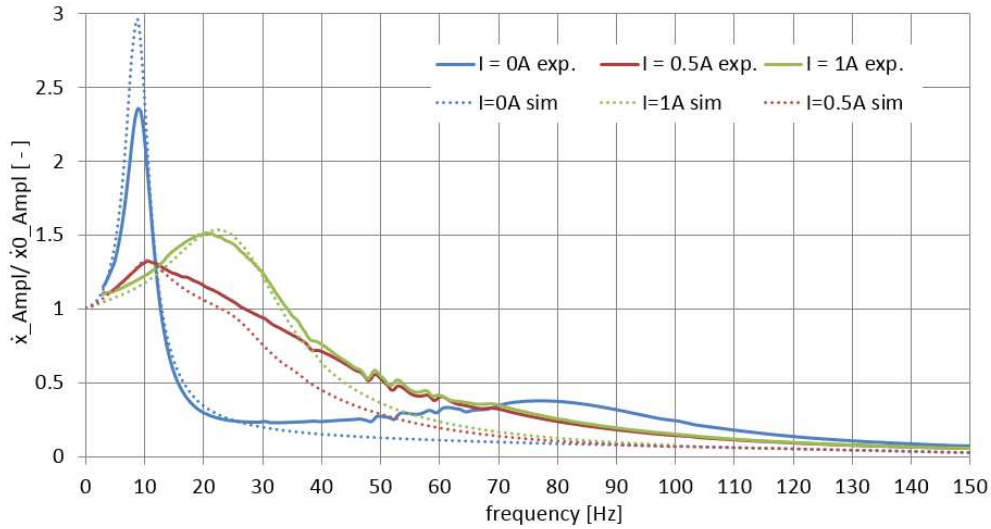

Fig. 26 Transfer ratio of a demonstrator with MR valve in passive mode

Simulated and measured data are not completely identical they differ primarily by a maximum of transfer ration with no current in the coil and the isolation properties at frequencies higher than *30 Hz*. This may be caused by passive losses of the real system (for example friction in linear bearings) which are not included in the model. However, there is one more difference, namely high damped peak around *80 Hz*, which disappears hand in hand with the current increase.

One of the possible causes of this transfer ratio increase is a so-called mass effect [13, 14]. That means the peak around *80 Hz* may be caused by oscillation of the fluid due to the elasticity of metal bellows (pressure thrust stiffness). This hypothesis was tested by additional measurements with various bellows or fluid, see chap. 5.3.4.

Semi-active control of the experimental strut have been investigated with the same excitation and the result was obtained by the same methods as in the case of passive mode. ON/OFF skyhook described by equation (2) was chosen as the control algorithm. However, the equation had to be modified for the real application: algorithm did not switch the damping force but the electric current in the coils of MR valve; an additional rule of the control was added to an acceleration noise elimination. The current in the coils valve coils was zero when the conditions (4) were not met.

$$(\dot{x} - \dot{x}_0) > 0.01 \wedge \dot{x} > 0.007 \quad \vee \quad (\dot{x} - \dot{x}_0) < -0.01 \wedge \dot{x} < -0.007 \tag{4}$$

1

$$\dot{x} \cdot (\dot{x} - \dot{x}_1) \geq 0 \rightarrow I = 1\ A$$

$$\dot{x} \cdot (\dot{x} - \dot{x}_1) < 0 \rightarrow I = 0\ A \tag{5}$$

0

$$I = 0\ A$$

Value of relative velocity *0.01 m/s* and *0.007 m/s* for the sprung mass velocity were obtained from several preliminary tests. Lower values of the velocities cause random switching of the current. Influence of the rule (4) is evident in Fig. 27, the relative velocity exceeds the value *0.01 m/s* sporadically for the excitation frequency *18 Hz* and higher. Therefore, there is a significant decrease in transfer ratio around the *18 Hz*.

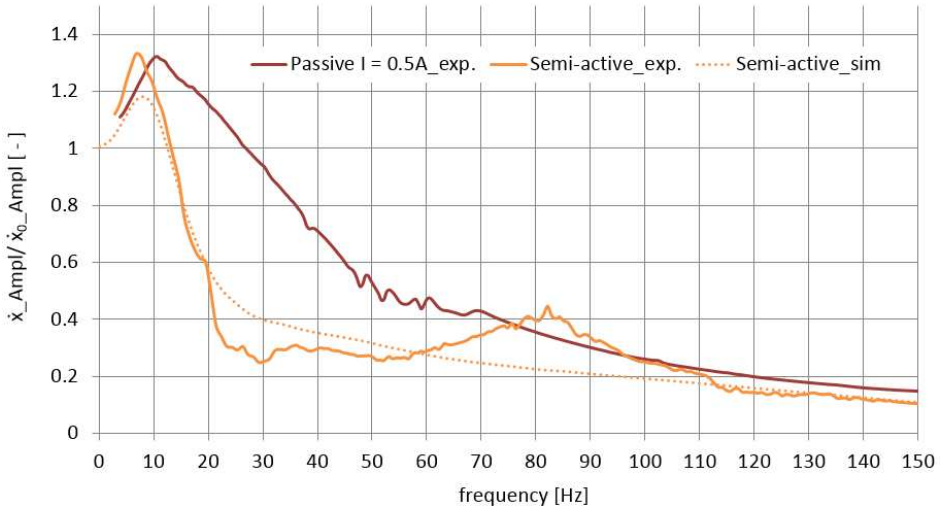

Fig. 27 Transfer ratio of a demonstrator with semi-active control of MR valve

The electric current in the MR valve coils was zero for the frequencies higher than *20 Hz* the resonance peak with a maximum around *80 Hz* appears in the semi-active controlled mode.

5.3.4 Conclusions of the experimental MR strut tests

Mass effect - a phenomenon described above may cause that the transfer ratio has a second resonance peak, in the case of Fig. 27 in the range between *50 – 110 Hz.* Hypothesis, that the peak is caused by a part of strut mass oscillation on a part of the strut stiffness was confirmed by re-measuring the transfer ratio with significantly stiffer bellows and a fluid with different density.

One of the possible causes of the peak is a movement of fluid mass m_f in the axial direction. The primary stiffness of strut k prevents this movement. However, in this case not only the axial deformation of bellows leads to the fluid flow, internal volume changes of bellows may cause the flow too. Resistant against this deformation is given by the sum of both bellows pressure thrust stiffness k_1

Bellows can change its shape by two different ways: length, volume. Total deformation is given by the combination of both ways. Resistance against this can be calculated as the sum of two spring's stiffness in series, mass is given by the volume calculations and known density the fluids.

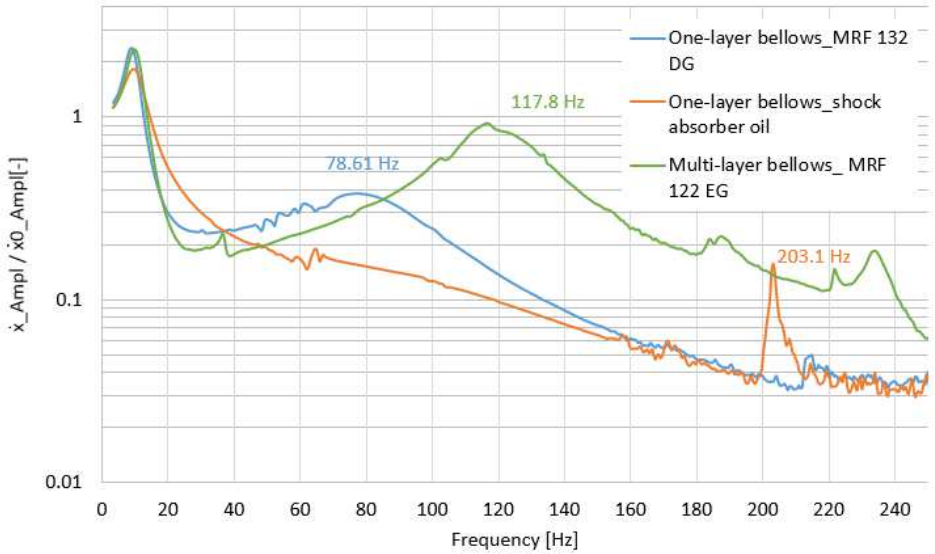

Fig. 28 Mass effect

tab. 2 Measured and calculated the modal frequency of the mass effect

Configuration	Counting [Hz]	Measurement [Hz]	Deviation [%]
Multi-layer, MRF 122 EG	146.9	117.8	25
Single-layer, MRF 132 DG	115.2	78.6	47
Single-layer, oil	209.6	203.1	3

Table 2 compares measured and calculated frequencies of modal shape, which may be caused by mass effect. This possible cause is supported by two facts: Firstly, an increase of damping causes disappearing of the phenomenon. Which is probably caused by the MRF yield stress increase in the gap and the fluid flow just by the bypass. This path exhibits much higher damping and the resonance peak is not reflected in the transfer ratio.

Secondly, a decrease of the fluid density results in a significant increase of the resonance frequency. However, the natural frequency calculated from a fluid mass differs from the measured resonance frequency.

The closed bypass was initially considered as an advantageous version for semi-active control, especially because of high dynamic force range at low relative velocities. However, ON state of MR valve exhibits a much higher transfer ratio than expected, see, Fig. 29. Therefore, the strut version without bypass was rejected.

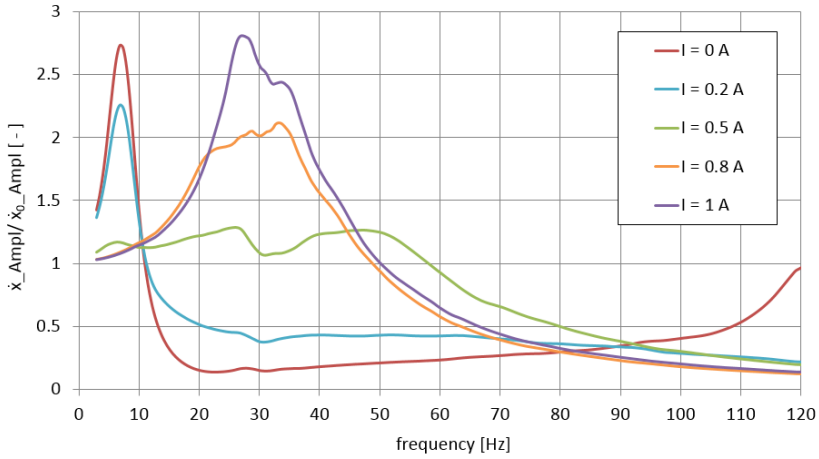

Fig. 29 Transfer ratio of a demonstrator with MR strut without bypass

This final design of strut will contain the bypass, which proposal is described in chap. 5.4.3 (hydraulic part).

Ferrite cracks were found after the tests with semi-active control. Wider rings (pos. 2) *t = 13 mm* has usually just chipped edges but the thinner *t = 4 mm* ring cracked totally (pos. 3). Therefore, its reuse was excluded.

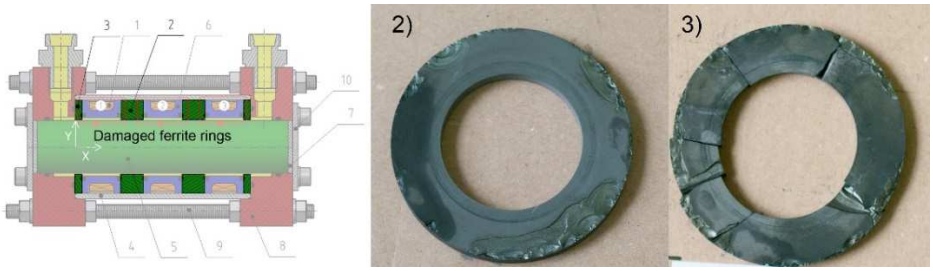

Fig. 30 Ferrite rings of MR valve after heavy loading

This accident started searching for another material, which guarantees a similar time response of MR valve, but it is more resistant to mechanical loads. Moreover, it will be advantageous that the new material will have higher saturation than the ferrite has. Vacoflux 50 the second has 4 times higher electrical resistivity than pure iron and almost 5 times higher saturation in comparison with ferrite. The electrical resistivity of material can be increased by suitable shape.

Therefore, research inspired by shape approach of eddy current elimination described in chap. 2.4.2 was started. Production technologies which were tested: glueing (a), grooving by wire cutting (b) 3D print (c) in Fig. 31.

Fig. 31 Shape approach of magnetic circuit time response decrease

The magnetic circuit of the final strut will make of Vacoflux 50, by 3D print using method SLM. Magnetic circuit time response decrease by shape approach is described in chap. 5.4.3 (magnetic part).

5.4 Design of the MR strut for VIS of the launch vehicle

5.4.1 Metal bellows design

Axial stiffness is commonly available in products list of bellows in contrast with the pressure thrust stiffness. Therefore, the FEM model was created to determination both stiffness based on the bellows geometry. Axial stiffness result is necessary for the model verification.

The model consists of two parts: wall (steel) and the fluid inside (oil). During the determination of axial stiffness, the fluid mesh is not considered in the model. The model was created in *ANSYS* software package as a plane model in *2D* using the rotational symmetry. The shell elements could not be used as in Thakkar thesis [18], because of the fluid and the wall interactions. But there is also mentioned the second approach – with solid elements with a note that the results of both methods do not differ significantly. Thus, the *SOLID 182* elements were used for the wall and *HSFLD 241* elements for fluid.

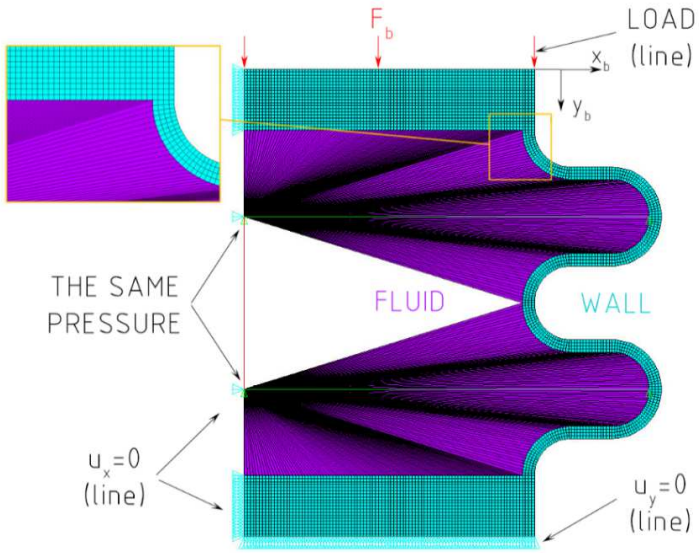

Fig. 32 FEM model of bellows

Load force is applied by the pressure on the top line, which corresponds to the force F_b. The displacement of the top line y_b is used for the stiffness calculation. The bottom line cannot move in vertical direction *Y*. Nodes located on Y axis cannot move in the horizontal direction *X*. There are several points (depends on a number of corrugations) with the same pressure in the mesh of fluid. It ensures identical pressure in the fluid, as shown in Fig. 32.

The FEM result of axial stiffness was compared with the measurement, counting carried out by the manufacturer and also with the value which is listed in the product list. The pressure thrust stiffness was compared just with the measurement described in chap. 5.3.2.

tab. 3 Bellows stiffness comparison determined by various methods

Procedure	Stiffness	Symbol	Value [N/mm]	Deviation [%]
Product list [33]	Axial	k_L	22.3	12.6
Manufacturer calc.	Axial	k_C	29.5	15.6
FEM model	Axial	k_F	25.52	ref. value
Measurement	Axial	k_M	22.7	11
FEM model	Press. th.	k_{1F}	1531.6	ref. value
Measurement	Press. th.	k_{1M}	1444.5	5.7

Sensitivity analysis of each parameter on the axial and pressure thrust stiffness was carried out after the model verification. The analysis uses the geometry of the bellows *324125*, just one dimension differs the tab. 11 to *90, 95, 105* a *110 %* of its initial value for each set of simulations.

The simulation results shows that some parameters have the same impact on both stiffnesses: *t, i, L;* while, two of them: D_m, *w* affected axial and pressure thrust stiffness differently, see Fig. 33. The conclusion of the sensitivity analysis is that the ratio between the pressure thrust and axial stiffness can be slightly modified by the geometry of the bellows. That may affect the ratio *N* between primary and secondary stiffness of the strut.

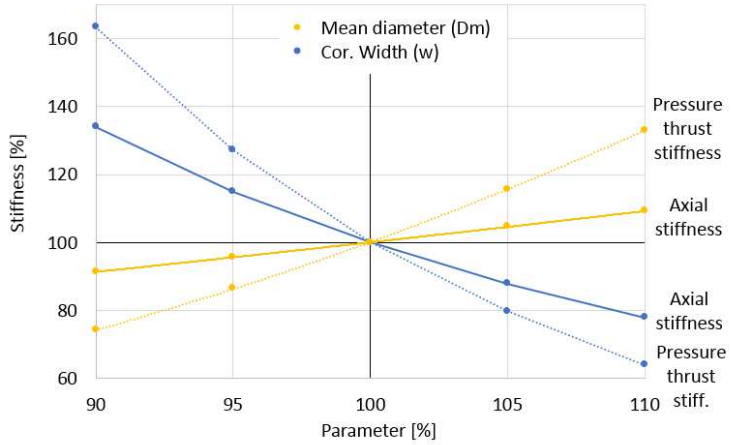

Fig. 33 Parameters with different impact to axial and pressure thrust stiffness

Verified model was used for select of suitable bellows for the strut with description *47.4x66x5x0.3* in [33]. Axial and pressure thrust stiffness was determined using the methodology described above. Ratio *N* between the primary and secondary stiffness was chosen as *N = 50.* Selected bellows and proposed axial stiffness of strut gives stiffness ratio:

$$N = \frac{k_B}{k_A} = \frac{k_{1b} * 2}{k_A} = \frac{23\,470 * 2}{1\,230} = 38.2 \qquad (6)$$

Considering that the FEA estimation of pressure thrust stiffness was *20%* lower than the measurement, the real ratio N should be higher. Anyway, change of *N* from 50 to 38 will not have a significant impact on VIS behaviour. However, the geometry modification of the chosen bellows that means custom made of the bellows should increase the ratio *N* to the required value.

5.4.2 Pneumatic spring design

Pneumatic spring is designed for a load of strut built in VIS with payload mass *1500 kg*. This load causes the equal pressure above and under piston of the pneumatic strut. The strut force-deformation dependency was determined by analytical counting; see Fig. 34. The strut stiffness is non-linear due to the pneumatic spring. The strut stiffness in steady state is:

$$k_A = K_p(0) + 2 \cdot k_b = 632.7 + 2 \cdot 298 = 1228.7 \quad (7)$$

This value is almost identical to the value used in the model. However, the strut force-deformation dependency has a progressive course of in compression part of the diagram and an almost linear course in tension. This feature is useful with respect to the flight direction (quasi-static acceleration).

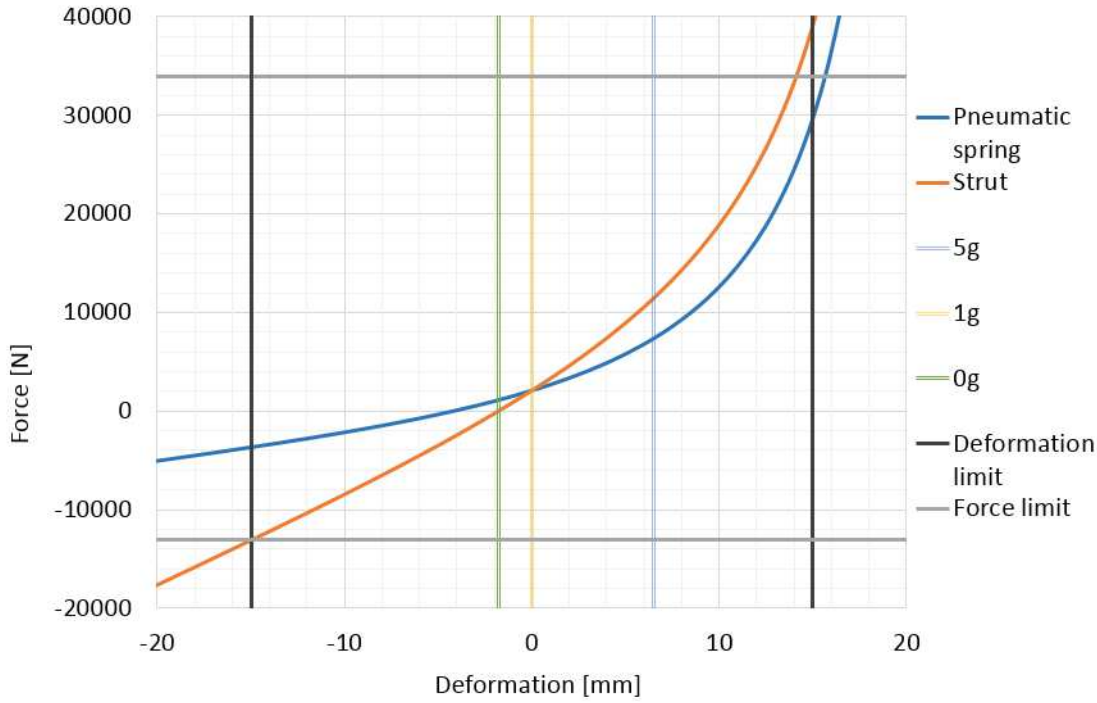

Fig. 34 Force-deformation dependency of the strut and its pneumatic spring

Progressive course of the strut force-deformation dependency allows decreasing of the maximal stroke of strut form *±20 mm* listed in onto *±15 mm*. This stroke reduction helps to decrease the weight of the strut.

5.4.3 MR valve design

MR valve design consisted of two models which are interconnected by several parameters, especially dimensions of the MR valve. The first one (hydraulic) is an analytical model of MR valve pressure drop causes by MR fluid flow through it. The second one (magnetic) is a FEM of the magnetic circuit which determines the yield stress of MR fluid in the gap.

Hydraulic part

An analytical model of MR fluid flow through gap or bypass, see Fig. 35 was created using the equation mentioned in [22]. The model determines pressure drop during the fluid flow, thus also damping force-velocity dependency.

The MR fluid flows via two paths: through the gap where the magnetic field can change of the fluid yield stress or through bypass orifice. Total flow rate *Q* has to be split into two parts *Q1*, *Q2*. The ratio between *Q1* and *Q2* depends on the intensity of the magnetic field in the gap and on the dimensions of channels. In the model, there is a rule that when the shear stress τ in the MR fluid is lower than the yield stress of MR fluid τ_f, then the *Q1* is zero.

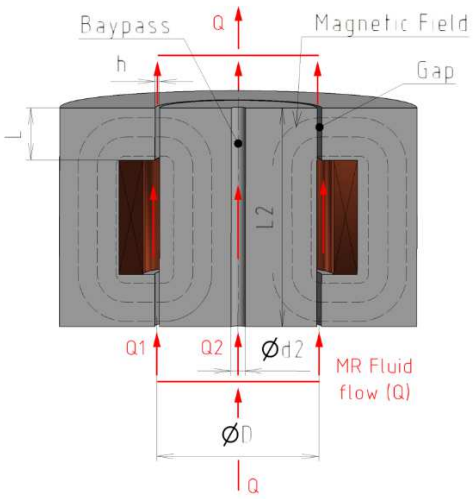

Fig. 35 MR valve hydraulic scheme

tab. 4 A combination of MR valve dimension meeting required F-v dependency

Dimension/Parameter	Symbol	Value	Unit
Gap thickness	h	0.65	[mm]
Gap length	L	22	[mm]
Gap mean diameter	D	42.65	[mm]
Bypass length	L2	40	[mm]
Bypass diameter	d2	1.95	[mm]

Dimensions mentioned in the tab. 4 ensures force-velocity dependencies in Fig. 36. The blue curve represents ON state, the orange one is for OFF state.

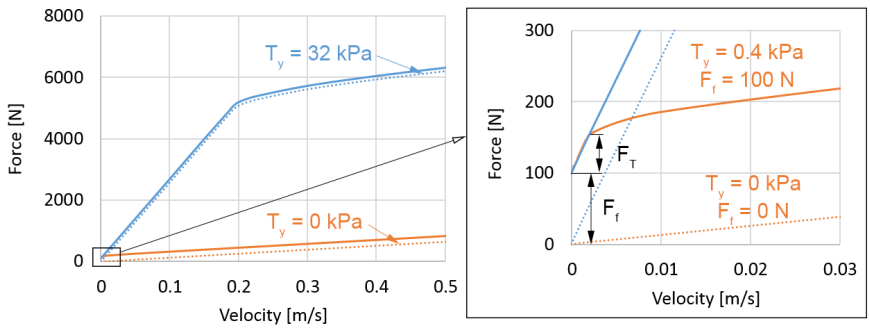

Fig. 36 The simulated F-v dependency of MR valve

The dynamic range of the strut with this MR damper will decrease by the friction of seals [34]. In the case of the MR strut, it will be the seal of pneumatic spring and guiding, which was estimated at *100 N*. Moreover, magnetic remanence of magnetic circuit material will cause a little yield stress even in the case of OFF state. The magnetic flux density in the gap of the magnetic circuit made of Vacoflux 50 was measured *15 mT* (measured on air – no MR fluid in the gap), this magnetic flux density causes *0.4 kPa* yield stress of *MRF 122 EG* [35]. Comparison of theoretical and predicted dynamic force range of MR strut for VIS of the launch vehicle is in Fig. 37.

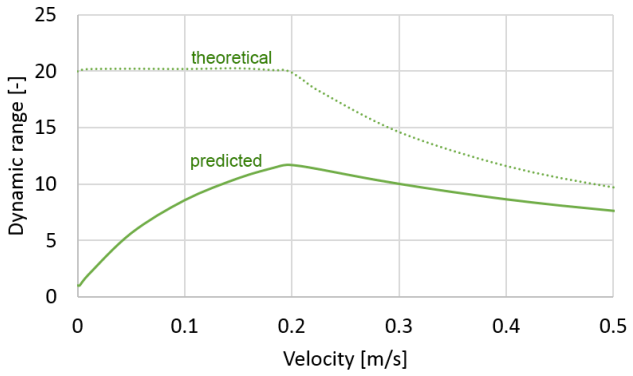

Fig. 37 MR strut dynamic force range

Magnetic part

Measured B-H curves Vacoflux and the MR fluid was inserted into the model using interpolation. The other materials used in the model was taken from libraries of the model software package – *ANSYS ELECTRONICS 2017* or from the product list.

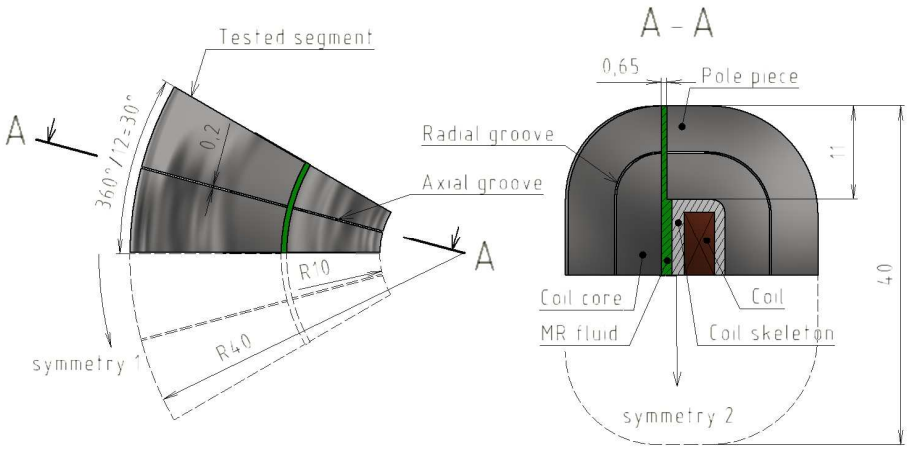

Fig. 38 Grooved magnetic circuit called as 24x2

Rotational symmetry (symmetry 1 in Fig. 38) was used, because of time-consuming simulations. Preliminarily results showed that the lowest number of grooves which gives satisfactory time response is 12, thereby circular sectors of the angle of 30° are created. The magnetic circuit is symmetrical around the horizontal plane (symmetry 2 in Fig. 38); therefore just half of the magnetic circuit was modelled. The example in Fig. 38 illustrates the circuit with 24 axial and 1 radial grooves, thereby 24x2 rods are created.

Shortening of time response was achieved by axial or the radial grooves. Under certain conditions the axial and radial groove has the same influence to time response, see *24x0* and *12x2* in Fig. 39. Substitution of the axial groove by the radial helps decreases the risk of saturation, which was observed in *96x0* version. Version *48x4* (Fig. 39) is characterized by shorter time response and higher intensity in the gap than the *96x0* version.

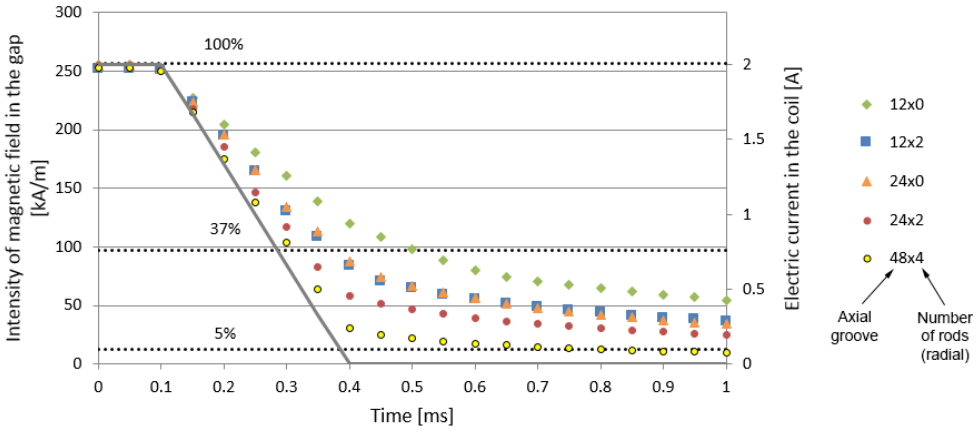

Fig. 39 Influence of grooves number to the time response

Grooves in axial and radial direction create rods of the magnetic circuit which cross section differs depending on the distance from the axis *Y*, see version 1 in the left side of Fig. 40. Thus, the magnetic field density is not constant in each rod, which is inappropriate due to the unnecessarily high weight of the magnetic circuit. Therefore, the shape of grooves and was modified, see Fig. 40. This figure compares magnetic flux density in three different magnetic circuits with the same excitation, constant current in the coil $I = 2A$ (simulation results for time $t = 0.05\ ms$).

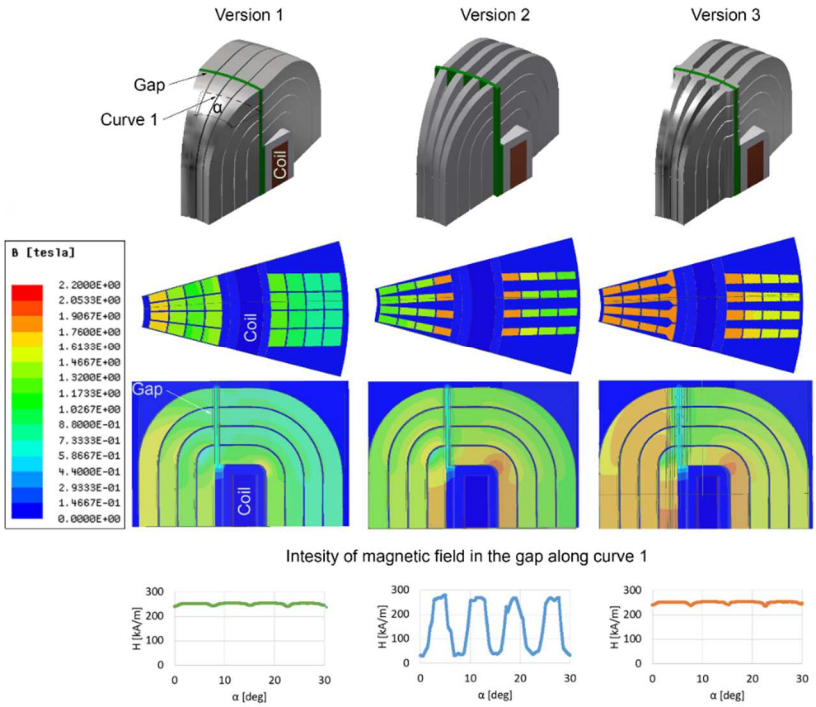

Fig. 40 Saturation of several versions of magnetic circuit excited by I = 2A (t = 0.05 ms)

Version 3 was chosen for the magnetic circuit in the MR strut. Primary time response is approximately *0.2 ms*. However, the time response of power supply is dominant in this value. Secondary time response is approximately *0.7 ms*. Time response of MR fluid (*0.5 ms*) must be added because it is not simulated in the transient model; thus, the time response of the MR valve is estimated at *1.2 ms*.

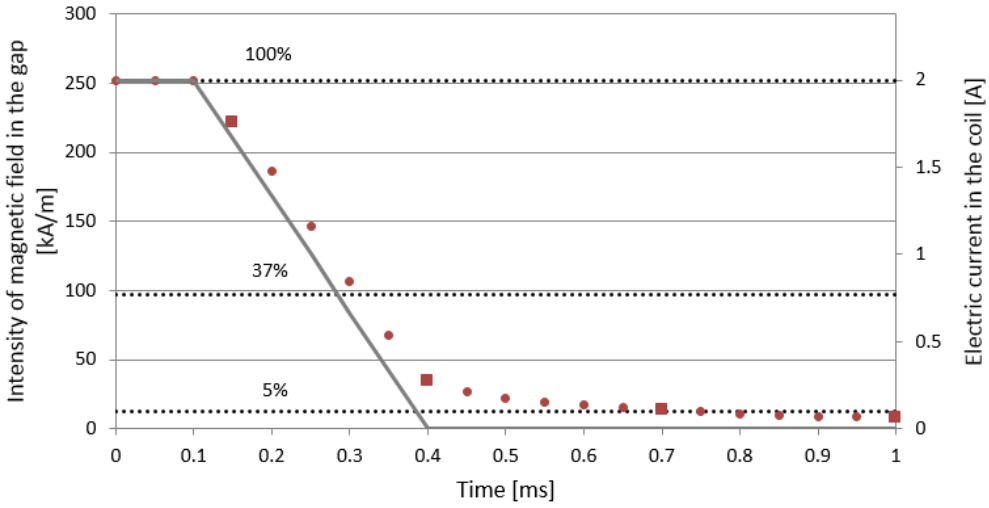

Fig. 41 Intensity of magnetic field in the gap of MR valve

Several points in Fig. 41 are marked by square; the magnetic flux density and the current density is plotted for these times in Fig. 42. Power supply disconnect causes a decrease of magnetic flux density in the magnetic circuit. However, eddy currents induce a secondary magnetic field; therefore, the magnetic flux density drop process is slowed down. Magnetic flux density in the final geometry dropped in coil core from *2* to *0.5 T* per *1 ms*.

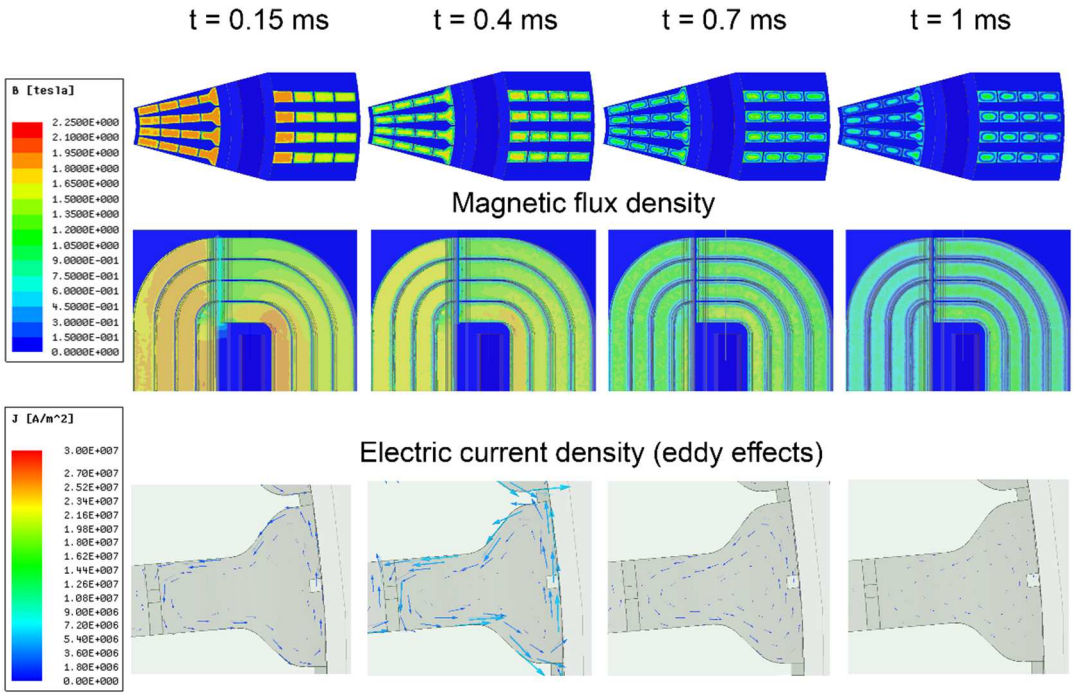

Fig. 42 Saturation of several versions of the mag. circuit (I = 2A, t = 0.05 ms)

The final version of magnetic circuit is grooved, see Fig. 43. When the grooves would be unfilled, the fluid could flow through them, so the bypass would be very high and the damping force of the MR valve would be very low. Therefore, the grooves will be filled with filled plastic.

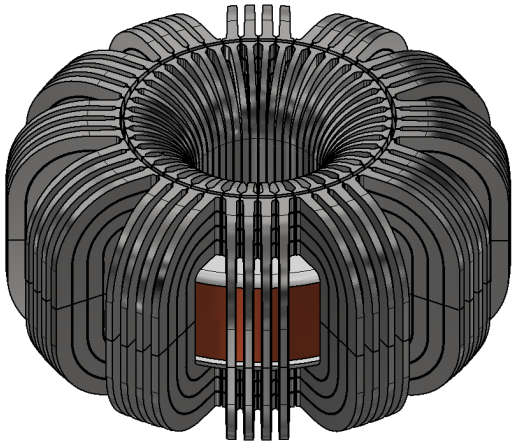

Fig. 43 Initial and final version of the magnetic circuit

5.4.4 Engineering design

The final structural design honours the division into two branches: damping (marked by shades of red in Fig. 44) and spring (shades of yellow). MR fluid is by the strut compression/extension forced to flow from one to another bellows through the MR valve which causes damping.

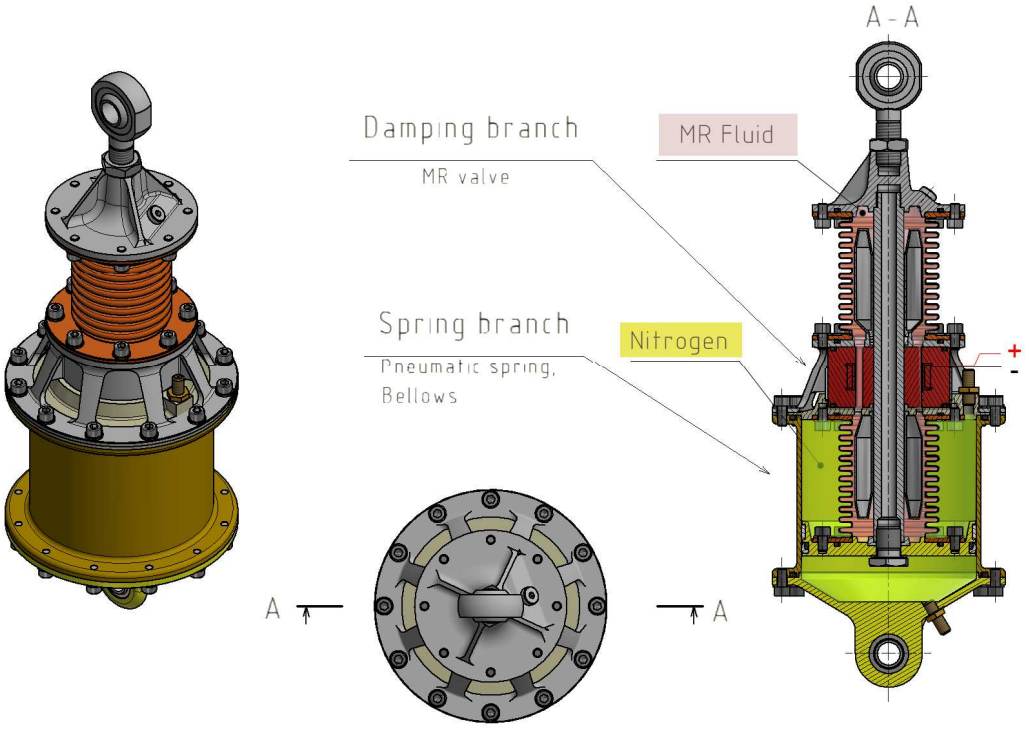

Fig. 44 MR strut branches

Dimensions of **MR valve** design is based on hydraulic and magnetic models described in chap. 5.4.3. The magnetic circuit of the MR valve consists of a coil wound on the skeleton which is surrounded by coil core and pole pieces. The pole pieces have to be dismountable, because of assembly (to insert the coil into the space in pole pieces). The pole pieces consist of 12 segments around the perimeter, which are divided onto 4x4 rods. Thus, a magnetic circuit consists of 196 rods.

The rods are interconnected by bridges, see the detail B in Fig. 45. These bridges are designed just because of manipulation after production. Influence of interconnection of rods by the bridges on time response of MR valve was tested in the magnetic model. The time response increase was negligible: *< 1%*.

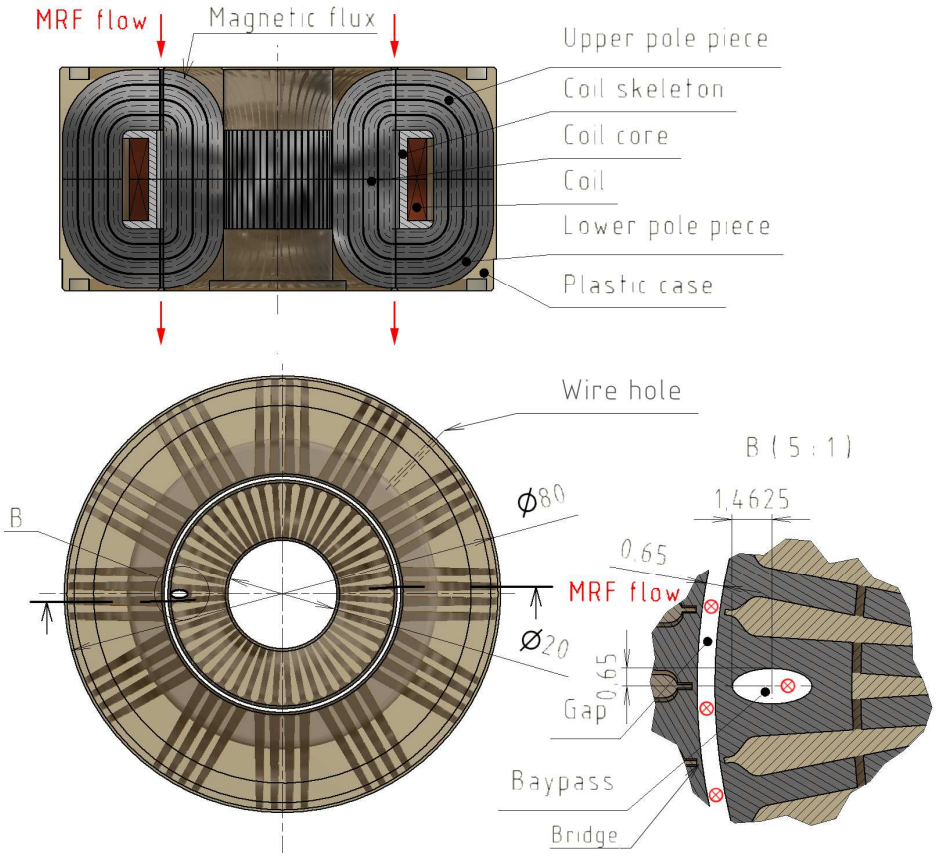

Fig. 45 Design of MR valve

The distance between connection eyes of the **MR strut** is *380 mm* in an equilibrium position. However, the length can be adjusted in the range of approximately *±2 mm* by the screw of the eye (pos. 19) and fixed by a nut (pos. 27). When the lower eye (pos. 20) is consider fixed, force loading of the upper eye causes an adapter (pos. 6) movement which is transferred to the piston of pneumatic spring (pos. 7) by a piston rod (pos. 8). Movement of the piston changes the pressure in the pneumatic spring chambers but also causes the bellows deformation (pos. 9). One of the bellows is compressed the other one is stretched, opposite faces of bellows are interconnected by the piston rod. That causes MR fluid flow through the MR valve (pos. 1), which is clamped between MR valve body (pos. 2) and flange (pos. 5) by screws M6 (pos. 22).

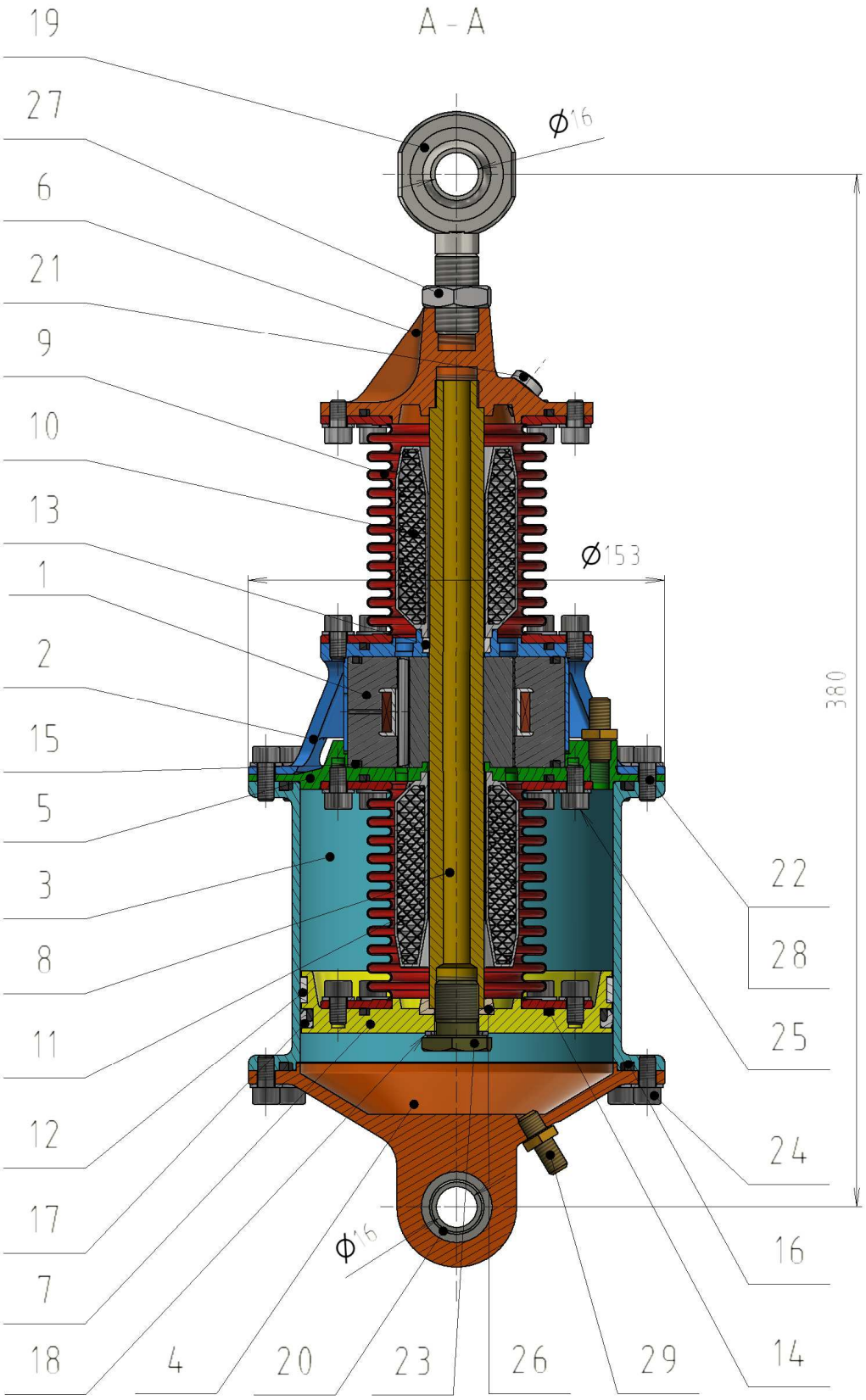

Fig. 46 Design of MR strut for VIS of the launch vehicle

Internal seals in the strut, for example in threads of the piston rod is not designed to leakage impossibility. Therefore, the threat of the piston rod is coated by sealant before thickening. These threats of piston rod fit in other parts: screw (pos. 23) or adapter which is as well as piston rod made of titanium, because of high stress in the threads. The screw connected piston rod and the piston, which is made of magnesium. Because of lower allowed compressive stress of magnesium, there is a washer (pos. 26) made of titanium between the piston and piston rod.

The total mass of MR strut was minimized by the sophisticated design of each part of the MR strut. Used material and weight of each component of MR strut is the tab. 5.

tab. 5 Comparison of an initial and final version of the magnetic circuit

Pos.	Name of part	Material	Weight [g]	Quantity
1	MR valve	Vacoflux / Lukopren / cooper /	693	1
2	MR valve body	AZ80A-T5 (magnesium alloy)	169	1
3	Cylinder	AZ80A-T5	337	1
4	Lid	AZ80A-T5	225	1
5	Flange	AZ80A-T5	159	1
6	Adapter	Ti6Al4V (titanium alloy)	279	1
7	Piston	AZ80A-T5	176	1
8	Piston rod	Ti6Al4V	230	1
9	Bellows	1.4571 (stainless steel)	447	2
10	Upper stopper	AZ80A-T5	49	1
11	Lower stopper	AZ80A-T5	48	1
12	Piston guideline	PTFE	2	1
13	Piston rod guideline	PTFE	11	1
14	Seal 66x2.5	NBR	1	4
15	Seal 71x2.5	NBR	2	2
16	Seal 123x3.4	NBR	4	2
17	Piston seal	NBR / PTFE	9	1
18	Bonded seal	NBR / Steel	2	1
19	Rod end M81935/1	Ti6Al4V	127	1
20	Lower eye MS14104	Ti6Al4V	16	1
21	Plug	AZ80A-T5 / NBR	2	1
22	Screw M6x16	Ti6Al4V	4	12
23	Piston rod screw	Ti6Al4V	23	1
24	Screw M6x12	Ti6Al4V	3	12
25	Screw M6x10	Ti6Al4V	3	32
26	Washer	Ti6Al4V	8	1
27	Nut	Ti6Al4V	12	1
28	Split washer 6.4	Ti6Al4V	0.4	56
29	Taxer valve	C-360 (brass alloy)	9	2

6 CONCLUSIONS

Vibration elimination in launch vehicle is specific in many factors: the vibration environment is quite hard and the frequency range is very wide. Any fluid fillings are allowed to be used only in case of their complete and reliable sealing. Finally, the weight of the vibration isolation system is very important factor in the assessment of the design. Previously designed VIS were summarized and divided into structural and mechanical groups. One of the mechanical VIS called ELVIS was chosen as an inspiration for this thesis and therefore, analysed to understand design background.

The strut of the VIS in this study consists of springs and magnetorheological damper enabling semi-active control of damping force. The benefit of semi-actively control in comparison to passive damping was proved by simulations of multi-body models. The models also served for the determination of the strut parameters and investigated their impact on the vibration elimination efficiency.

The simulations with the semi-active algorithm ON/OFF skyhook have shown that the most significant factor of semi-actively controlled dampers is their time response. The lower time response the damper exhibits the lower transmissibility of vibrations can be achieved by VIS equipped by this damper. Dynamic force range increase (in this case increased by OFF state damping drop) causes a slight increase of the transmissibility in the vicinity of resonance but the significant drop of the transmissibility in the isolation area.

The requirement of perfect sealing of the MR strut for VIS of the launch vehicle was solved by the use of elastic metal bellows sealed by static seals as the only possible way of safe sealing. A damper with elastic bellows used for the damping medium case must be considered elastically connected. The stiffness of the connection is affected by the resistance of the bellows length changes against the internal pressure increase – pressure thrust stiffness.

The pressure thrust stiffness is not a commonly available parameter of the bellows. Therefore, the FEA of bellow filled with a fluid was provided and verified by measurement in this thesis. Moreover, sensitivity analysis revealed that the mean diameter of damper and width of corrugation affects axial and pressure thrust stiffness differently. Thus, the ratio between axial and pressure thrust stiffness of bellows can be adjusted by these two parameters of bellows.

Two versions of MR strut were designed in this study, one of them: the experimental MR strut was also manufactured and tested. This test provided valuable knowledg which was used in the final MR strut design for the VIS of launch vehicle.

One of the most important findings was that the elastic bellows allow an oscillations of MR fluid which appears as a peak in the transfer function. This phenomenon is called fluid mass effect and its future research could help to clarify the reason why the resonance frequency is not dependent only on the mass of a fluid and the stiffness of bellows.

The magnetic circuit made of ferrite was damaged during testing of the experimental strut. The ferrite rings cracked because of strong force impulse occurring during vibration elimination by semi-actively controlled MR damper. This material is not suitable for parts of the magnetic circuit which are loaded by a force. Therefore, a new way of very fast magnetic circuit designing has been investigated in this study – shape approach.

The main aim of shape approach, as well as the material approach of fast magnetic circuit design, is the eddy currents elimination. A magnetic circuit with suitably designed grooves can achieve similar time response as the circuit made of a material with very low electrical conductivity (for example the ferrite). Moreover, a material with a higher level of saturation can be used for shape approach. This results in a significant weight reduction of the magnetic circuit.

The magnetic circuit of the MR strut of VIS for the launch vehicle is made of Vacoflux 50. The magnetic circuit contains 48 grooves in the axial direction (created circular sectors) and 4 radial grooves (parallel to magnetic flux). Both types of grooves together created 192 rods of the magnetic circuit which are electrically isolated by grooves filled with plastic. This design of magnetic circuit exhibits primary time response (step from *100* to *32.7 %* of damping force) of *0.2 ms* and secondary response (step from *100* to *5 %* of damping force) of around *0.7 ms* in the case of the electrical current drop takes *0.3* ms from *2 A* onto *0 A*. Estimated secondary time response of the MR strut with this magnetic circuit is *1.2 ms* (containing the MR fluid time response itself).

The grooved magnetic circuit is also very efficient in terms of weight. The MR strut designed with an external MR valve made of ferrite had nearly twice the mass in comparison with the grooved magnetic circuit of the MR strut. Both mentioned struts were designed for the same loading. Nevertheless, the weight penalty in comparison of less efficient but lighter passive adapters will be probably acceptable only for transport of extremely sensitive payloads. However, the MR strut can be applied in other fields of vibration isolation, where the weight is not the decisive factor.

7 LITERATURE

[1] The Price of Space, 2018. News from the Galactic Centre [online]. New Zealand [cit. 2018-08-14]. Link: https://milky-way.kiwi/2018/01/25/the-price-of-space/

[2] DAVIS, L. P., J. F. WILSON and R. E. JEWELL, 1986. Hubble Space Telescope Reaction Wheel Assembly Vibration Isolation System. Alabama, Arizona: National Aeronautics and Space Administration.

[3] Ariane 6, M's old blog [online]. [cit. 2018-08-23]. Link: http://armchairengineer.blogspot.com/2014/02/ariane-6-where-does-it-come-from-and.html

[4] EILERS, D. a A. RITTWEGER. LPDR Study Executive Summery Report. Bremen, 2007. Link: http://esamultimedia.esa.int/docs/gsp/completed/C16812ExS.pdf

[5] RUEBSAMEN, D. T., 2003. Evolved launch vibration isolation system (ELVIS) demonstration unit test results. In: Proc. of the 2003 S/C and L/V dynamics Environments Workshop, The Aerospace Corporation. El Segundo: California, s.

[6] WILKE, P, C JOHNSON, P GROSSERODE and D SCIULLI, 2000. Whole-spacecraft vibration isolation for broadband attenuation. In: 2000 IEEE Aerospace Conference. NEW YORK, USA: IEEE, 315-321.

[7] WHITE, J., E. FOWLER a K. NOBLE, 2015. SoftRide® Shock and Vibration Isolation Systems. In: 2nd Workshop on Spacecraft Shock Environment and Verification.

[8] PEREZ, E. Ariane 5: User's Manual. Paris, 2011.

[9] PAYLOAD ADAPTER. EADS CASA [online]. Espacio: Opinio, 2013 [cit. 2016-05-23]: http://www.casaespacio.es/products/payloadadapter.

[10] ANDERSON, E.H., D. J. LEO, M. D. HOLCOMB and I. CHOPRA, 1996. Ultraquiet platform for active vibration isolation. SMART STRUCTURES AND INTEGRATED SYSTEMS. 1996-5-1, 1996(2717), 436-451. DOI: 10.1117/12.239046.

[11] LEE, D.O., G. PARK a J.H. HAN, 2015. Experimental study on on-orbit and launch environment vibration isolation performance of a vibration isolator using bellows and viscous fluid. Aerospace Science and Technology. 45, 1-9. DOI: 10.1016/j.ast.2015.04.012. ISSN 12709638.

[12] CHI, W., D. CAO, D. WANG, J. TANG, Y. NIE and W. HUANG, 2015. Design and Experimental Study of a VCM-Based Stewart Parallel Mechanism Used for Active Vibration Isolation. Energies. 8(8), 8001-8019. DOI: 10.3390/en8088001. ISSN 1996-1073.

[13] DAVIS, P., D. CUNNINGHAM and J. HARRLER. Advanced 1.5 Hz Passive Viscous Isolation System. In: Adaptive Structures Forum. Reston, Virigina: American Institute of Aeronautics and Astronautics, 1994, -. DOI: 10.2514/MASF94.

[14] BOYD, James, H, Timothy, A HINDLE, Tristram, T HYDE and David, A OSTERBERG. A viscous isolation and damping strut utilizing a fluid mass effect. WO2005095822 A1. 2005-10-06.

[15] Images, 2014. Metalic Bellows [online]. Vettuvankeni Village, India [cit. 2018-06-20]. http://www.metallicbellows.org/images/DSC_0545-big.jpg.

[16] KUMAR, J. P. N., S. J. KUMAR, R. K. S. JEYATHILAK, M. VENKATESH, A. S. CHRISTOPHER and K. C. GANESH, 2017. Effect of design parameters on the static mechanical behaviour of metal bellows using design of experiment and finite element analysis. International Journal on Interactive Design and Manufacturing (IJIDeM). 11(3), 535-545. DOI: 10.1007/s12008-016-0306-7.

[17] FARAJI, G., M. K. BESHARATI, M. MOSAVI and H. KASHANIZADEH, 2008. Experimental and finite element analysis of parameters in manufacturing of metal bellows. The International Journal of Advanced Manufacturing Technology. 38(7-8), 641-648. DOI: 10.1007/s00170-007-1122-9. ISSN 0268-3768.

[18] THAKKAR, H. R. Study of design aspects of expansion joints with metallic bellows and their performance evaluation. Sardar Patel University, 2011. Supervisor: George,P. M.

[19] Pressure Thrust, 2005. Hyspan [online]. Hyspan Precision Products [cit. 2018-06-20]. http://www.hyspan.com/pdfs/PressureThrustNotes.pdf.

[20] WINSLOW, W. M., 1949. Induced Fibration of Suspensions. Journal of Applied Physics. 20(12), 1137-1140. DOI: 10.1063/1.1698285. ISSN 0021-8979.

[21] HANLON, M., Audi's new magnetic semi-active suspension system. Automtive [online]. 2006 [cit. 2018-06-20]. https://newatlas.com/go/5752/.

[22] YANG, G., B.F. SPENCER, J.D. CARLSON and M.K. SAIN. Large-scale MR fluid dampers: modeling and dynamic performance considerations. Engineering Structures. 2002, vol. 24(3): 309-323. DOI: 10.1016/S0141-0296(01)00097-9. ISSN 01410296.

[23] SPENCER Jr. BF, YANG G, CARLSON JD andSAIN MK. Smart dampers for seismic protection of structures: a full-scale study. In: Proceedings of 2nd World Conference on Structural Control, vol. 1, Kyoto, Japan, 1998. p. 417–26.

[24] GONCALVES F., KOO J. H. and AHMADIAN M. 2003 Experimental approach for finding the response time of MR dampers for vehicle applications DETC 2003 19th Biennial Conf. on Mechanical Vibration and Noise (Chicago, IL, Sept. 2003).

[25] STRECKER, Z., I. MAZŮREK, J. ROUPEC and M. KLAPKA, 2015. Influence of MR damper response time on semiactive suspension control efficiency. Meccanica. 50(8), 1949-1959. DOI: 10.1007/s11012-015-0139-7. ISSN 0025-6455.

[26] KOO, J. H., F. D. GONCALVES and M. AHMADIAN, 2006. A comprehensive analysis of the response time of MR dampers. Smart Materials and Structures. 15(2), 351-358. DOI: 10.1088/0964-1726/15/2/015. ISSN 0964-1726.

[27] SAHIN, H., N. M. WERELEY, R. TAO, F. GORDANINEJAD, X. WANG and Y. LIU, 2012. Response time of magnetorheological fluids and magnetorheological valves under various flow conditions. Journal of Intelligent Material Systems and Structures. 23(9), 949-957. DOI: 10.1177/1045389X12447984. ISSN 1045-389X.

[28] BEWLEY, L. V. and H. PORITSKY, 1937. Intersheet Eddy-Current Loss in Laminated Cores. Transactions of the American Institute of Electrical Engineers. 56(3), 344-346. DOI: 10.1109/T-AIEE.1937.5057543. ISSN 0096-3860.

[29] FIORILLO, F., C. BEATRICE, O. BOTTAUSCIO and E. CARMI, 2014. Eddy-Current Losses in Mn-Zn Ferrites. IEEE Transactions on Magnetics. 50(1), 1-9. DOI: 10.1109/TMAG.2013.2279878. ISSN 0018-9464.

[30] MUKERJI, S. K., M. GEORGE, M. B. RAMAMURTHY and K. ASADUZZAMAN, 2008. Eddy Currents in Laminated Rectangular Cores. Progress In Electromagnetics Research. 83, 435-445. DOI: 10.2528/PIER08062101. ISSN 1559-8985.

[31] P/M Parts, ©2018. Sumitomo Electrics [online]. Sumitomo Electric Industries [cit. 2018-06-20]. http://global-sei.com/pmp/product_e/seihin01_eng.html.

[32] KELSO, J. and E. LINDER. Magnetorheological Fluid Vibration Isolator. US20040195061 A1. 2004-10-07.

[33] Metal Bellows Manual, 2002. Witzenmann [online]. Pforzheim [cit. 2018-06-20]. https://www.witzenmann.de/en/media/Metal_bellows_manual_0441e_02_04_10_20_download.pdf.

[34] MACHÁČEK, O.; KUBÍK, M.; MAZŮREK, I.; STRECKER, Z.; ROUPEC, J. Frictionless Bellows Unit Connected with the Magnetorheological Valve. In ENGINEERING MECHANICS 2016. First edition, 2016. Praha: Institute of Thermomechanics Academy of Sciences of the Czech Republic, 2016. s. 354-357. ISBN: 978-80-87012-59- 8.

[35] MRF-122EG, 2015. LORD MR Store [online]. Mid Atlantic Rubber [cit. 2018-06-20]. http://www.lordmrstore.com/lord-mr-products/mrf-122eg-magneto-rheological-fluid.